View Article Online / Journal Homepage / Table of Contents for this issue

A series of transition metal–azido extended complexes with various anionic and neutral co-ligands: synthesis, structure and their distinct magnetic behavior†

Oindrila Sengupta, Bappaditya Gole, Sandip Mukherjee and Partha Sarathi Mukherjee*

Received 22nd March 2010, Accepted 14th May 2010
First published as an Advance Article on the web 9th July 2010
DOI: 10.1039/c0dt00181c

Published on 09 July 2010 on http://pubs.rsc.org | doi:10.1039/C0DT00181C
Downloaded by University of Chicago on 22/04/2013 15:54:28.

The crystal structures and magnetic properties of five new transition metal–azido complexes with two anionic [pyrazine-2-carboxylate (pyzc) and *p*-aminobenzoate (paba)] and two neutral [pyrazine (pyz) and pyridine (py)] coligands are reported. All five complexes were synthesized by solvothermal methods. The complex $[Co_2(pyzc)_2(N_3)_2(H_2O)_2]_n$ (**1**) is 1D and exhibit canted antiferromagnetism, while the 3D complex $[MnNa(pyzc)(N_3)_2(H_2O)_2]_n$ (**2**) has a complicated structure and is weakly ferromagnetic in nature. $[Mn_2(paba)_2(N_3)_2(H_2O)_2]_n$ (**3**), is a 2D sheet and the Mn^{II} ions are found to be antiferromagnetically coupled. The isostructural 2D complexes $[Cu_3(pyz)_2(N_3)_6]_n$ (**4**) and $[Cu_3(py)_2(N_3)_6]_n$ (**5**) resemble remarkably in their magnetic properties exhibiting moderately strong ferromagnetism. Density functional theory calculations (B3LYP functional) have been performed to provide a qualitative theoretical interpretation of the overall magnetic behavior shown by these complexes.

Introduction

The fascinating hybrid organic–inorganic coordination assemblies have engrossed considerable attention at the forefront of synthetic material science.[1] This surge has been primarily motivated by their intriguing structural diversity[2] and, more recently, from their potential applications in many fields such as gas storage, ion exchange, catalysis, and magnetism.[3] Remarkably, the most widely employed synthetic strategy is the solvo(hydro)thermal method inherited from zeolite chemistry. The structures may be varied or tailored by introducing different auxiliary ligands. The diversity of coordination and supramolecular chemistry and the powerful tool of crystal engineering, enabled the chemists in this field to obtain many new magnetic materials, for example, the newly-emerged single-molecule and single-chain magnets.[4,5] Additionally, these materials have offered great opportunities to better understand fundamental magnetic phenomena, such as long-range ordering (LRO), spin canting, metamagnetism, anisotropy, relaxation dynamics, and quantum tunneling of magnetization.[5a] As far as LRO is concerned, some complex and exotic behaviors have been revealed in molecular systems, for example, the presence of multiple areas of bistability or multi-stepped hysteresis,[6] and the combination of magnetic properties and other functions.[7]

In this sense, a plethora of azido-bridged magnetic systems have been well characterized, accompanied by considerable magneto–structural studies from both experimental and theoretical viewpoints.[8–14] The strong coordination tendency with transition metals and the various bridging abilities of this pseudohalide anion provide numerous advantages for constructing homometallic or heterometallic magnetic architectures with various structural characteristics, and it is possible to control the spatial arrangement of azido-bridged complexes by the suitable choice of the cationic templates or capping organic ligands. An interesting strategy towards high-dimensional framework derivatives is to incorporate a second bridging ligand into the metal–azido systems.[8–10] As for the compounds reported to date, most of the coligands are neutral organic ligands, while charged ligands are relatively less used.[12] Synthesizing high-dimensional compounds with azide and negative ligands presents a challenge for researchers of this topic. Commonly, it is difficult for two different kinds of negative ligands to coexist in the same molecule because of their competition in the process of self-assembly.

Many examples of transition metal–azido systems with carboxylate ligands have been reported.[15] However, because of the possibility of explosion, the azide must be handled carefully; thus, as an efficient synthetic method, hydrothermal reaction has seldom been applied in the synthesis of such complexes. It is worth mentioning that when azido ligands coordinate to M^{II} ions in either μ-1,1 or μ-1,1,1 modes it normally mediates ferromagnetic coupling. Thus, it is a challenge to design new structural features for maintaining the ferromagnetic coupling by introducing other functions into metal–azido complexes. Pyrazine-2-carboxylate (pyzc) is a particularly interesting co-ligand in the sense that if both the nitrogen atoms coordinate to two different metal centers, it ensures an extended structural motif that can be further extended using the azido bridges. To the best of our knowledge only one such mixed valent copper complex is known in the literature[16] and here we report two new complexes, $[Co_2(pyzc)_2(N_3)_2(H_2O)_2]_n$ (**1**) and $[MnNa(pyzc)(N_3)_2(H_2O)_2]_n$ (**2**). We also used *p*-aminobenzoate (paba) in view that it also has two coordinating sites *para* to each other and isolated a third complex $[Mn_2(paba)_2(N_3)_2(H_2O)_2]_n$ (**3**). An intrepid attempt of using excess amounts of the azide ligand with copper and pyzc in solvothermal synthesis was made and we

Department of Inorganic and Physical Chemistry, Indian Institute of Science, Bangalore, 560012, India. E-mail: psm@ipc.iisc.ernet.in; Fax: 91-80-23601552; Tel: 91-80-22933352

† Electronic supplementary information (ESI) available: Diagrams representing the topological networks, Curie–Weiss fitting of the $1/\chi_M$ *vs.* *T* data of all five complexes and atomic spin densities of complexes **4** and **5**. CCDC reference numbers 770739–770743. For ESI and crystallographic data in CIF or other electronic format see DOI: 10.1039/c0dt00181c

Published on 09 July 2010 on http://pubs.rsc.org | doi:10.1039/C0DT00181C
Downloaded by University of Chicago on 22/04/2013 15:54:28.

were able to isolate a new copper complex, $[Cu_3(pyz)_2(N_3)_6]_n$ (**4**), that resulted from the decarboxylation of pyzc ligand. However, attempts to synthesize the same complex using only pyrazine instead of pyzc as a starting material were not successful in either room temperature or hydrothermal conditions. But we were able to isolate an isostructural copper complex with pyridine again under solvothermal conditions, $[Cu_3(py)_2(N_3)_6]_n$ (**5**). Here we report the synthesis, crystal structures and variable temperature magnetic properties of these five new complexes with some theoretical calculations (DFT) in support of the experimental magnetic data.

Experimental

Materials

$Co(NO_3)_2{\cdot}6H_2O$, $MnCl_2{\cdot}4H_2O$, $Cu(NO_3)_2{\cdot}3H_2O$, pyrazine-2-carboxylic acid, *p*-aminobenzoic acid, NaN_3 and solvents employed were commercially available and used without further purification. Elemental analyses of C, H, and N were performed using a Perkin-Elmer 240C elemental analyzer. IR spectra were recorded as KBr pellets using a Magna 750 FT-IR spectrophotometer. The variable temperature magnetic studies in the range of 2–300 K were carried out on crystalline samples using a Quantum Design MPMS-XL5 SQUID magnetometer. The experimental susceptibility data were corrected for diamagnetism (Pascal's tables).[4b]

Synthesis of complex $[Co_2(pyzc)_2(N_3)_2(H_2O)_2]_n$ (1). To an aqueous solution of pyrazine-2-carboxylic acid (62 mg, 0.5 mmol) and $Co(NO_3)_2{\cdot}6H_2O$ (291 mg, 1 mmol), sodium azide (390 mg, 6 mmol) was added and the resulting deep pink solution was placed in a 23 ml Teflon-lined hydrothermal flask and was heated at 140 °C for 30 h. After slow cooling of the solution to room temperature over a period of 10 h brown plate shaped X-ray quality crystals of **1** were collected and dried under vacuum. Isolated yield: 35% (based on cobalt). Anal. Calcd for **1**, $C_{10}H_{10}Co_2N_{10}O_6$: C, 24.81; N, 28.93; H, 2.08. Found: C, 24.83; N, 28.60; H, 2.15. IR (cm^{-1}): 2079 (N_3^-), 1660 (COO^-).

Caution! *Although we did not experience any problems with the compounds reported in this work, azido complexes of metal ions in the presence of organic ligands are potentially explosive. Only a small amount of material should be prepared, and it should be handled with care.*

Synthesis of complex $[MnNa(pyzc)(N_3)_2(H_2O)_2]_n$ (2). An aqueous solution of NaN_3 (390 mg, 6 mmol) was added to a mixture of pyrazine-2-carboxylic acid (62 mg, 0.5 mmol) and $MnCl_2{\cdot}4H_2O$ (198 mg, 1 mmol). The resulting yellow solution was kept in a 23 ml Teflon-lined hydrothermal flask and was heated at 140 °C for 30 h. Slow evaporation of the resulting solution at room temperature gave rise to needle shaped yellow crystals after 5 days which were collected by filtration, washed with methanol and dried. Isolated yield: 40% (based on manganese). Anal. Calcd for **2**, $C_5H_7MnN_8NaO_4$: C, 18.70; N, 34.89; H, 2.19. Found: C, 19.02; N, 34.66; H, 1.88. IR (cm^{-1}): 2091 (N_3^-), 1665 (COO^-).

Synthesis of complex $[Mn_2(paba)_2(N_3)_2(H_2O)_2]_n$ (3). To a methanolic solution of *p*-aminobenzoic acid (68 mg, 0.5 mmol) and $MnCl_2{\cdot}4H_2O$ (198 mg, 1 mmol), NaN_3 was added (130 mg, 2 mmol). The resulting yellow solution was transferred to a 23 ml Teflon-lined hydrothermal flask and was heated at 160 °C for 24 h. After completion of the reaction it produces a red solution, slow evaporation of which gave red plate shaped crystals after 10 days. The crystals were washed with methanol and dried. Isolated yield: 36% (based on manganese). Anal. Calcd for **3**, $C_7H_8MnN_4O_3$: C, 33.47; N, 22.31; H, 3.20. Found: C, 33.78; N, 22.04; H, 3.46. IR (cm^{-1}): 2090 (N_3^-), 1598 (COO^-).

Synthesis of complex $[Cu_3(pyz)_2(N_3)_6]_n$ (4). An aqueous solution of $Cu(NO_3)_2{\cdot}3H_2O$ (243 mg, 1 mmol) was added to a pyrazine-2-carboxylic acid (62 mg, 0.5 mmol) taken in water. A brown precipitate was formed on addition of aqueous NaN_3 solution (390 mg, 6 mmol) to the metal solution. The whole mixture was transferred in a 23 ml Teflon-lined hydrothermal flask and was heated at 140 °C for 30 h. On slow evaporation of the filtrate gave rise to black needle shaped crystals which were washed with methanol and dried. Isolated yield: 60% (based on copper). Anal. Calcd for **4**, $C_8H_8Cu_3N_{22}$: C, 15.93; N, 51.10; H, 1.33. Found: C, 15.70; N, 50.87; H, 1.32. IR (cm^{-1}): 2092 (N_3^-).

Synthesis of complex $[Cu_3(py)_2(N_3)_6]_n$ (5). A brown precipitate was obtained on addition of NaN_3 (390 mg, 6 mmol) to a mixture of $Cu(NO_3)_2{\cdot}3H_2O$ (243 mg, 1 mmol) and pyridine (40 mg, 0.5 mmol) taken in aqueous medium. The resulting solution was placed in a 23 ml Teflon-lined hydrothermal flask and was heated at 140 °C for 30 h. On cooling slowly to room temperature gave rise to black plate shaped crystals suitable for X-ray analysis. Isolated yield: 55% (based on copper). Anal. Calcd for **5**, $C_{10}H_{10}Cu_3N_{20}$: C, 19.98; N, 46.60; H, 1.67. Found: C, 19.82; N, 46.40; H, 1.52. IR (cm^{-1}): 2092 (N_3^-).

X-Ray crystallographic data collection and refinements†

Single crystal X-ray data were collected on a Bruker SMART APEX CCD diffractometer using the SMART/SAINT software.[17] Intensity data were collected using graphite-monochromatized Mo-Kα radiation (0.71073 Å) at 293 K. The structures were solved by direct methods using the SHELX-97[18] program incorporated into WinGX.[19] Empirical absorption corrections were applied with SADABS.[20a] Hydrogen atoms were located wherever possible. All non-hydrogen atoms were refined with anisotropic displacement coefficients. The hydrogen atoms bonded to carbon were included in geometric positions and given thermal parameters equivalent to 1.2 times those of the atom to which they were attached. Structures were drawn using ORTEP-3 for Windows.[20b] The crystallographic refinement parameters are listed in Table 1.

Network analysis is emerging as an important tool in understanding the actual structural pattern of complicated coordination polymers. The Schläfli symbol for **1** to **3** obtained by using the programme TOPOS4.0[21] was $(4^2.6)$ with 3-c net (uninodal net), $(3^4.4^4.5^2)(3^5.4^7.5^8.6)$ with (5-c)(7-c) 2-nodal net and $(3^2.4^2.5^2)(3^4.4^4.5^4.6^3)$ with (4-c)(6-c) 2-nodal net respectively. Similarly the isostructural complexes **4** and **5** contain the Schläfli symbol $(3^6.4^2.5^6.6)(3^9.4^9.5^3)^2$ with (6-c)(7-c)^2 2-nodal net. The perspective views of the topologies for all the complexes are given in the supporting information (Fig. S1, ESI†).

Computational methodology

The following computational methodology was used to calculate the exchange coupling constants in the reported complexes.[22–25] Using a phenomenological Heisenberg Hamiltonian

 This journal is © The Royal Society of Chemistry 2010

Table 1 Crystallographic data and refinement parameters for **1–5**

Identification code	**1**	**2**	**3**	**4**	**5**
Formula	$C_{10}H_{10}Co_2N_{10}O_6$	$C_5H_7MnN_8NaO_4$	$C_7H_8MnN_4O_3$	$C_8H_8Cu_3N_{22}$	$C_{10}H_{10}Cu_3N_{20}$
Formula weight	484.12	317.06	249.09	602.94	600.96
Temperature/K	293(2)	293(2)	293(2)	293(2)	293(2)
Wavelength	0.71073	0.71073	0.71073	0.71073	0.71073
Crystal system	Triclinic	Monoclinic	Triclinic	Monoclinic	Monoclinic
Space group	$P\bar{1}$	$C2/c$	$P\bar{1}$	$P2_1/n$	$P2_1/n$
a/Å	7.0638(6)	20.8162(14)	7.4957(7)	11.9395(6)	11.9024(8)
b/Å	7.1293(6)	15.7305(12)	7.5942(7)	6.0952(3)	6.0183(2)
c/Å	8.1458(6)	7.7103(5)	9.4664(8)	15.2200(9)	14.8927(11)
α/°	103.861(7)	90	83.198(1)	90	90
β/°	95.840(7)	110.499(3)	73.133(1)	111.266(3)	110.524(9)
γ/°	102.916(7)	90	62.105(1)	90	90
V/Å^3	382.94(6)	2364.9(3)	455.67(7)	1032.19(9)	999.08(11)
Z	2	8	2	2	2
ρ_c/g cm^{-3}	2.099	1.804	1.830	1.940	1.998
μ/mm^{-1}	2.228	1.179	1.440	3.113	3.214
F(000)	242.0	1288.0	254.0	594.0	594.0
Unique reflns	2131	3595	2122	3126	2889
GOF (F^2)	1.067	1.083	1.048	1.033	0.979
R_1[a]	0.0427	0.0492	0.0265	0.0324	0.0452
wR_2[b]	0.1337	0.1331	0.0674	0.0785	0.1092

[a] $R_1 = \sum\|F_o\| - |F_c\|/\sum|F_o|$. [b] $wR_2 = [\sum\{w(F_o^2 - F_c^2)^2\}/\sum\{w(F_o^2)^2\}]^{1/2}$.

Published on 09 July 2010 on http://pubs.rsc.org | doi:10.1039/C0DT00181C
Downloaded by University of Chicago on 22/04/2013 15:54:28.

$H = -\sum J_i S_j S_k$ (where i labels the different kind of coupling constants, while j and k refer to the different paramagnetic centers) to depict the exchange coupling between each pair of transition-metal ions present in the polynuclear complex, the full Hamiltonian matrix for the entire system can be constructed.

The hybrid B3LYP functional[26] has been used in all calculations as implemented in the *Gaussian 03* package,[27] mixing the exact Hartree–Fock-type exchange with Becke's expression for the exchange functional[28] and that proposed by Lee–Yang–Parr for the correlation contribution.[29] The use of the non-projected energy of the broken-symmetry solution as the energy of the low-spin state within the DFT framework provides more or less satisfactory results avoiding the cancellation of the non-dynamic correlation effects.[30] The broken symmetry approach along with electron correlations at the B3LYP level has been widely used to investigate magnetic properties in a large number of magnetic systems. We have used the LANL2DZ basis set for all of the atoms. All of the energy calculations were performed including 10^{-8} density-based convergence criterion.

Results and discussion

Synthesis

The solvothermal methods have been widely used to synthesize new materials and especially the carboxylate based polynuclear coordination architectures. But due to the potentially explosive nature of azide, the reactions with this ligand must be carried out with utmost care. Our cautious attempt to use excess of NaN_3 and that at relatively higher temperatures (>130 °C) was very successful and we were able to isolate five new and novel polynuclear metal–azido complexes. The relative amounts of the various reactants, solvents, and the reaction conditions were optimized after several unsuccessful attempts. The final compositions of the materials are quite different than their starting compositions, but the reported procedures are highly reproducible. Complex **4** was formed accidentally by high temperature decarboxylation of pyrazine-2-carboxylic acid and a synthesis of the same product starting with pyrazine itself was not successful in room temperature or under solvothermal conditions. Interestingly complex **5** which is structurally equivalent to complex **4**, was readily synthesized by the solvothermal method form pyridine itself as the starting material.

The IR spectra of complexes **1**, **2** and **3** show characteristic carboxylic stretching frequencies (υ_{asym} C=O) at 1660, 1665 and 1598 cm^{-1} respectively. Additionally they also show the very intense azido peaks at 2079, 2090 and 2091 cm^{-1} respectively. Complexes **4** and **5** show the most intense azido peak at the same frequency of 2092 cm^{-1}.

Structure description of $[Co_2(pyzc)_2(N_3)_2(H_2O)_2]_n$ (1)

A perspective view of a fragment of this 1D complex is given (Fig. 1) and selected bond parameters are summarized in Table 2. The complex crystallizes in the triclinic space group $P\bar{1}$, with two formulae/unit cell. The structure of this complex contains one unique Co atom, one unique azido group, one unique pyrazine-2-carboxylate group and one coordinated water molecule. The metal atom has a distorted octahedral geometry with two nitrogen atoms [N(1)] from two EO-azido groups in *cis*-positions [Co(1)–N(1), 2.131(3) Å and Co(1)–N(1), 2.172(3) Å], and one oxygen atom of a coordinated water molecule [Co(1)–O(3 W), 2.002(3) Å] and one carboxylato oxygen atom [Co(1)–O(1), 2.100(2) Å] *trans* to the two azido nitrogen atoms. The other two sites are taken up by two aromatic nitrogen atoms from two different pyrazine-2-carboxylate ligands [Co(1)–N(4), 2.124(3) Å, Co(1)–N(5), 2.196(3) Å]. The neighboring metal atoms [Co(1)–Co(1)] are connected by double EO-bridging azido ligands forming the

Published on 09 July 2010 on http://pubs.rsc.org | doi:10.1039/C0DT00181C
Downloaded by University of Chicago on 22/04/2013 15:54:28.

Table 2 Selected bond lengths (Å) and angles (°) for complexes **1**, **2** and **3**

1					
Co(1)–O(3W)	2.082(3)	Co(1)–O(1)	2.100(2)	Co(1)–N(4)	2.124(3)
Co(1)–N(1)	2.131(3)	Co(1)–N(1)$^{\#1}$	2.172(3)	Co(1)–N(5)	2.196(3)
O(3W)–Co(1)–O(1)	98.64(11)			O(3W)–Co(1)–N(4)	87.02(11)
O(1)–Co(1)–N(4)	77.34(10)			O(3W)–Co(1)–N(1)	98.23(12)
O(1)–Co(1)–N(1)	160.04(11)			N(4)–Co(1)–N(1)	92.99(11)
O(3W)–Co(1)–N(1)$^{\#1}$	171.32(11)			O(1)–Co(1)N(1)$^{\#1}$	88.06(10)
N(4)–Co(1)–N(1)$^{\#1}$	99.91(11)			N(1)–Co(1)–N(1)$^{\#1}$	76.32(13)
O(3W)–Co(1)–N(5)	86.19(11)			O(1)–Co(1)–N(5)	98.81(10)
N(4)–Co(1)–N(5)	171.60(10)			N(1)–Co(1)–N(5)	92.86(11)
N(1)$^{\#1}$–Co(1)–N(5)	87.33(11)				
Symmetry transformations used to generate equivalent atoms: #1 $-x$, $-y$, $-z$.					
2					
Mn(1)–N(1)	2.306(2)	Mn(1)–O(1)	2.159(2)	Mn(1)–N(3)$^{\#1}$	2.174(2)
Mn(1)–O(3)	2.264(2)	Mn(1)–N(3)	2.279(3)	Mn(1)–N(6)	2.146(3)
Na(1)–O(3)	2.420(2)	Na(1)–N(8)$^{\#2}$2.427(3)	Na(1)–O(4)	2.387(3)	
Na(1)–N(5)$^{\#3}$	2.462(3)	Na(1)–O(4)$^{\#4}$	2.469(3)	Na(1)–N(6)	2.547(3)
N(6)–Mn(1)–O(1)	97.19(10)			N(6)–Mn(1)–N(3)$^{\#1}$	101.99(11)
O(1)–Mn(1)–N(3)$^{\#1}$	158.68(9)			N(6)–Mn(1)–O(3)	86.33(9)
O(1)–Mn(1)–O(3)	88.72(8)			N(3)$^{\#1}$–Mn(1)–O(3)	101.62(8)
N(6)–Mn(1)–N(3)	97.20(10)			O(1)–Mn(1)–N(3)	158.68(9)
N(3)$^{\#1}$–Mn(1)–N(3)	79.77(10)			N(1)–Mn(1)–N(3)	90.94(9)
N(1)–Mn(1)–Na(1)	127.47(6)			O(1)–Mn(1)–Na(1)	101.49(6)
N(3)$^{\#1}$–Mn(1)–Na(1)	141.58(7)			N(3)–Mn(1)–Na(1)	98.62(7)
O(4)–Na(1)–O(3)	86.04(8)			O(4)–Na(1)–N(8)	99.93(12)
O(3)–Na(1)–N(8)	160.76(13)			N(5)–Na(1)–O(4)	158.02(12)
O(3)–Na(1)–N(5)	78.18(11)			N(8)–Na(1)–N(5)	99.96(14)
O(4)–Na(1)–N(6)	94.50(10)			O(3)–Na(1)–N(6)	74.78(8)
Symmetry transformations used to generate equivalent atoms: #1 $-x+1/2$, $-y+1/2$, $-z$ #2 x, $-y$, $z-1/2$ #3 x, y, $z-1$ #4 $-x+1$, y, $-z-1/2$.					
3					
Mn(1)–N(1)	2.2107(14)	Mn(1)–O(1)	2.2230(12)	Mn(1)–N(4)	2.3273(15)
Mn(2)–O(2)	2.0824(12)	Mn(2)–N(1)	2.2438(14)	Mn(2)–O(1W)	2.2828(16)
N(1)$^{\#1}$–Mn(1)–N(1)	180.0			N(1)–Mn(1)–O(1)$^{\#1}$	88.12(5)
N(1)–Mn(1)–O(1)	91.88(5)			O(1)$^{\#1}$–Mn(1)–O(1)	180.0
N(1)$^{\#1}$–Mn(1)–N(4)$^{\#2}$	93.63(6)			N(1)–Mn(1)–N(4)$^{\#2}$	86.37(6)
O(1)$^{\#1}$–Mn(1)–N(4)$^{\#2}$	94.56(5)			O(1)–Mn(1)–N(4)$^{\#2}$	85.44(5)
N(4)$^{\#2}$–Mn(1)–N(4)$^{\#3}$	180.0			O(2)–Mn(2)–O(2)$^{\#4}$	180.0
O(2)–Mn(2)–N(1)	90.33(5)			O(2)$^{\#4}$–Mn(2)–N(1)	89.67(5)
N(1)–Mn(2)–N(1)$^{\#4}$	180.0			O(2)–Mn(2)–O(1W)$^{\#4}$	90.42(6)
N(1)–Mn(2)–O(1W)$^{\#4}$	93.17(6)			O(2)–Mn(2)–O(1W)	89.58(6)
N(1)–Mn(2)–O(1W)	86.83(6)				

Symmetry transformations used to generate equivalent atoms: #1 $-x+1$, $-y$, $-z$ #2 x, y, $z+1$ #3 $-x+1$, $-y$, $-z-1$ #4 $-x$, $-y+1$, $-z$.

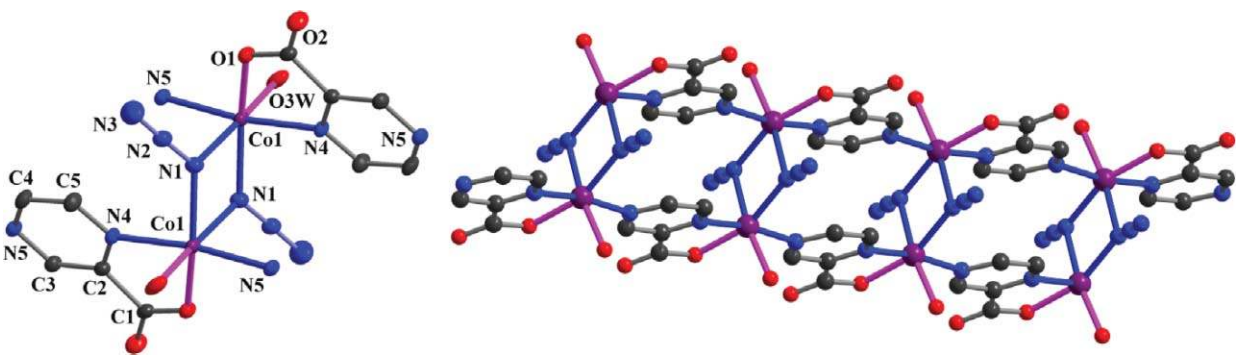

Fig. 1 Thermal ellipsoid probability (30%) view with atom numbering scheme of the basic unit (left) and the 1D structure (right) of complex **1**. Hydrogen atoms have been removed for clarity.

basic dinuclear structure, which, in turn, are joined together by the *trans* nitrogen atoms of pyrazine-2-carboxylate to give the overall 1D chain structure running along the crystallographic *a*-axis. The azido group thus acts as an end-on and the pyrazine-2-carboxylate acts as a $\mu_{N,N,O}$-donor ligand. Within the dinuclear units the Co(1)–N(1)–Co(1) angle measured to be 103.68°.

Structure description of $[MnNa(pyzc)(N_3)_2(H_2O)_2]_n$ (2)

It has a complicated 3D heterometallic structure as shown in Fig. 2. The basic unit of the complex (Fig. 3) consists of one Mn(II), one Na(I), two azido anions, one pyrazine-2-carboxylate anion and two coordinated water molecules. The two neighboring Mn(II) ions are

 This journal is © The Royal Society of Chemistry 2010

Published on 09 July 2010 on http://pubs.rsc.org | doi:10.1039/C0DT00181C
Downloaded by University of Chicago on 22/04/2013 15:54:28.

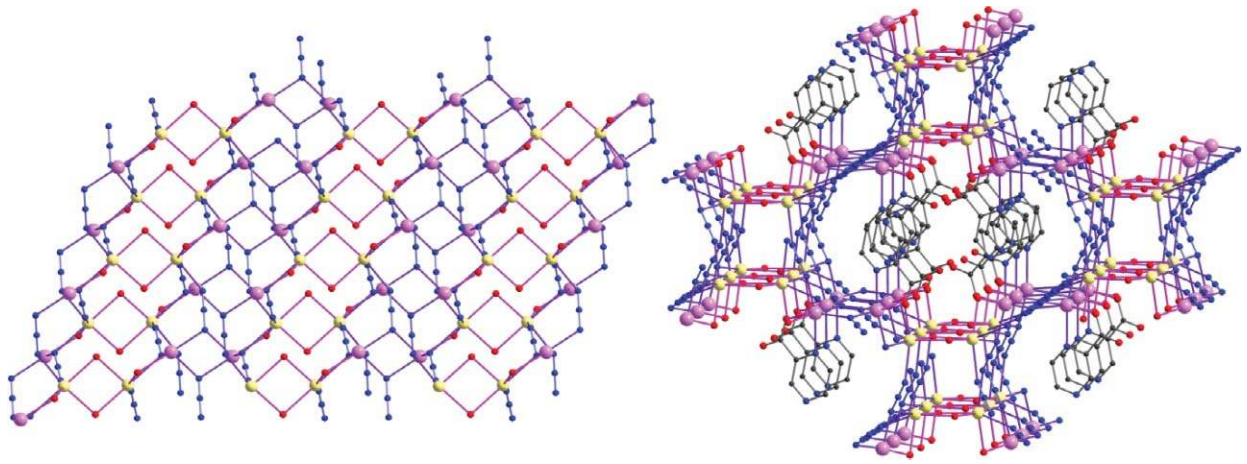

Fig. 2 A view of the 3D framework of **2** along the crystallographic *b*-axis (left, the pyzc ligands have been omitted for clarity) and along a slightly tilted *c*-axis (right). Color code: Mn – pink, Na – yellow, C – grey, N – blue and O – red.

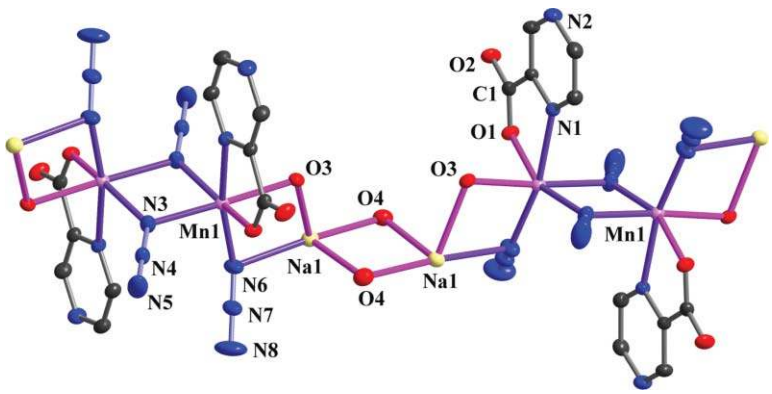

Fig. 3 Thermal ellipsoid probability (30%) view with atom numbering scheme of the basic fragment of **2**. Hydrogen atoms have been removed for clarity.

linked together by two EO-azido bridges [Mn(1)–Mn(1), 3.42 Å], which are joined to two Na(1) atoms [Mn(1)–Na(1), 3.56 Å] on both sides by a single EO-azido and a μ_2-bridging oxygen atom [O(3)] from a water molecule. The two nearest Na atoms [Na(1)–Na(1), 3.55 Å] are connected to each other by two oxygen atoms from two water molecules, giving an spiral chain like structure of alternating Mn_2 and Na_2 motifs. These chains are held together in space by μ_3-bridging azido groups. One of these azido groups joins two Mn atoms and a Na atom acting as a $\mu_{1,1,3}$,η^2-ligand and the other one joins one Mn with two Na atoms utilizing the same bridging mode, with a difference that in the second case it joins two different metals in EO-fashion. Interestingly, the pyrazine-2-carboxylate does not act as a bridging ligand, providing just two coordinating atoms [N(1) and O(1)] to the Mn(II) ion (Fig. 2).

The geometry around the Mn atom is roughly octahedral, with four nitrogen and two oxygen atoms in its coordination sphere. One carboxylato oxygen atom [Mn(1)–O(1), 2.159(2) Å] and one water oxygen atom [Mn(1)–O(3), 2.264(2) Å] are in *cis* disposition to each other. The three azido nitrogen atoms occupy one of the faces of the octahedron [Mn(1)–N_{EO}, 2.146(3)–2.279(3) Å] and the aromatic nitrogen atom [Mn(1)–N(1), 2.306(2) Å] is *trans* to one of the azido nitrogen atom [N(6)]. The Na atoms are also six-coordinate in nature with three water oxygen atom and three azido nitrogen atoms occupying opposite faces of a rough octahedron. The Na–O bonds range from 2.387 Å to 2.469 Å and Na–N bonds range from 2.427(3) Å to 2.547(3) Å. The Mn(1)–N(3)–Mn(1) and Mn(1)–N(6)–Na(1) angles measure at 100.23° and 98.19° respectively.

Structure description of $[Mn_2(paba)_2(N_3)_2(H_2O)_2]_n$ (3)

As illustrated in Fig. 4, the structure of **3** contains two unique Mn atoms, one unique azido anion, one unique 4-aminobenzoate anion and one coordinated water molecule. Both the Mn atoms have a roughly octahedral geometry. The Mn(2) atom has two equivalent set of bonds with two azido nitrogen atoms [N(1)] and two carboxylate oxygen atoms [O(2)] in a plane and *trans* to each other [Mn(2)–N(1), 2.2438(14) Å, Mn(2)–O(2), 2.0824(12) Å]. The other two positions are occupied by two oxygen atoms [O(1W)] from two water molecules again *trans* to each other [Mn(2)–O(1W), 2.2828(16) Å]. The other metal atom [Mn(1)] also has a similar coordination environment of two sets of bonds with two azido nitrogen atoms [Mn(1)–N(1), 2.2107(14) Å] and two carboxylato oxygen atoms [Mn(1)–O(1), 2.2230(12) Å] arranged in a plane *trans* to each other. But the remaining two axial positions are taken up by two amino nitrogen atoms [Mn(1)–N(4), 2.3273(15) Å]. The nearest Mn atoms joined with each other by single $\mu_{1,1}$-azido and $\mu_{1,3}$-carboxylato bridges forms a 1D chain which are again joined with each other by the amino groups of 4-aminobenzoate to give an overall 2D network. So the azido

Published on 09 July 2010 on http://pubs.rsc.org | doi:10.1039/C0DT00181C
Downloaded by University of Chicago on 22/04/2013 15:54:28.

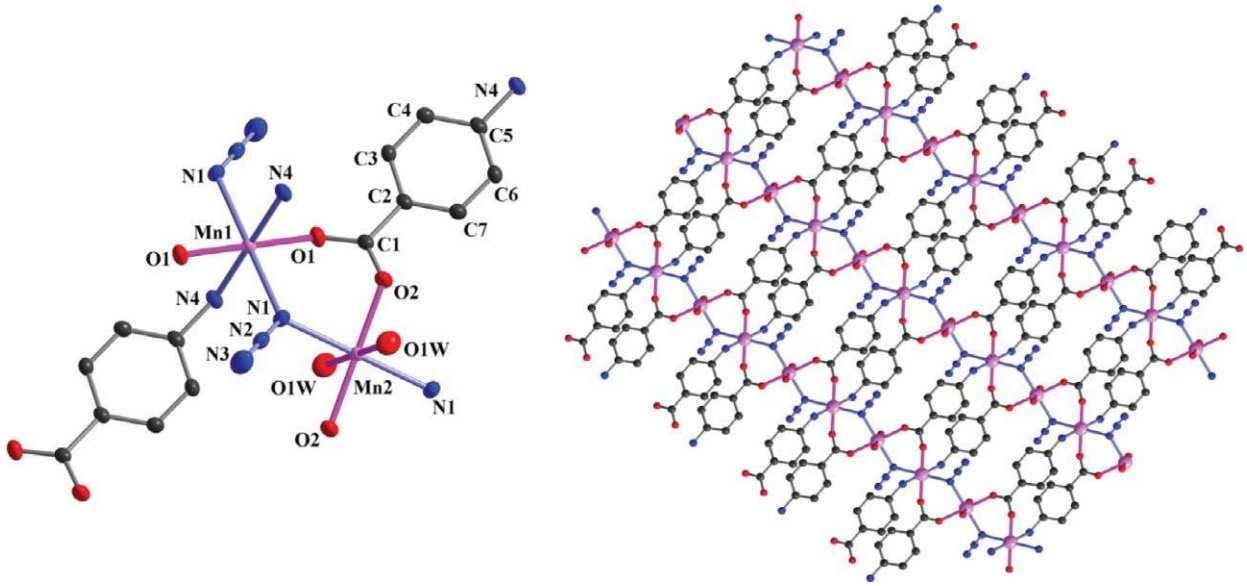

Fig. 4 Thermal ellipsoid probability (30%) view with atom numbering scheme of the basic unit (left) and the 2D structure (right) of **3**. Hydrogen atoms have been removed for clarity.

groups acting as μ_2,η^1-bridges joins two Mn atoms, while the 4-aminobenzoate group bridges three Mn atoms in μ_3,η^3-fashion. Within the chains the Mn(1)–N(1)–Mn(2) angle, that is, the angle involving the EO-azido group measures at 121.79°.

To the best of our knowledge, only one more Mn-complex is known with these two anionic ligands together, $[Mn(4\text{-aba})N_3]_n$, that lacks the coordinated water molecules and having a different structure with nearest Mn atoms joined by double EO-azido bridges.[31]

Structure description of $[Cu_3(pyz)_2(N_3)_6]_n$ (4) and $[Cu_3(py)_2(N_3)_6]_n$ (5)

Compound **4** is a complicated 2D coordination assembly built from centrosymmetric trinuclear $[(pyz)(N_3)Cu(\mu_{1,1}\text{-}N_3)_2Cu(\mu_{1,1}\text{-}N_3)_2Cu(N_3)(pyz)]$ units which are linked by the two $\mu_{1,1,3}$-azido groups linked to two terminal Cu^{II} atoms (Fig. 5). Important interatomic distances and angles are given in Table 3. The central Cu(2) atom sitting on an inversion center has an elongated octahedral geometry around it. The four equatorial short bonds [Cu(2)–N(4), 1.9954(19) Å and Cu(2)–N(7), 1.9905(19) Å] are formed by a set of two double end-on azido bridges linking it to the two terminal Cu(1) atoms. The elongated sites are taken up by two nitrogen atoms [N(3)] of the triply-bridging azido groups of two different trinuclear units which join them together [Cu(2)–N(3), 2.622 Å]. The terminal Cu(1) atoms adopt a square-pyramidal geometry with two $\mu_{1,1}$-azido ligands in *cis* orientation [Cu(1)–N(4), 2.0194(19) Å; Cu(1)–N(7), 2.002(2) Å], one $\mu_{1,1,3}$-azido [Cu(1)–N(1), 2.0214(19) Å] and a nitrogen atom of the pyz ligand [Cu(1)–N(10), 1.9975(19) Å] in the basal plane along with a nitrogen atom of a triply bridging azido group in the apical position [Cu(1)–N(3), 2.517 Å]. Each of the trinuclear units are thus linked to two neighboring units by a set of two Cu(1)–N(3)–Cu(2) bridges along the crystallographic *b*-axis, and with two others by Cu(1)–N(1)–N(2)–N(3)–Cu(2) bridges across the *ac*-plane to give a 2D coordination polymer. Within the trinuclear units the adjacent Cu^{II} atoms are at a distance of about 3.09 Å. The $[Cu(\mu_{1,1}\text{-}N_3)_2Cu]^{2+}$ core in **4** is symmetric with four short bonds and two corresponding Cu–N–Cu angles measure at 100.47° and 101.25°.

Complex **5** is isostructural with complex **4** (Fig. 6), and a detailed description of its structure is thus not necessary. Table 3 illustrates the bond parameters of these two complexes and they are remarkably similar.

To the best of our knowledge, there are six other structurally characterized Cu^{II} complexes known in the literature that have a related trinuclear unit. Three of them, namely, $[Cu_3(N_3)_6(Meinic)_2(DMF)_2]_n$,[32] $[Cu_3(N_3)_6(ampym)_2(DMF)_2]_n$,[33]

Table 3 Selected bond lengths (Å) and angles (°) for complexes **4** and **5**, in the **4**/**5** format

Cu(1)–N(10)	1.9975(19)/1.994(3)	Cu(1)–N(7)	2.002(2)/1.994(3)
Cu(1)–N(4)	2.0194(19)/2.013(3)	Cu(1)–N(1)	2.0214(19)/2.020(3)
Cu(2)–N(4)	1.9954(19)/1.999(3)	Cu(2)–N(7)	1.9905(19)/1.984(3)
N(10)–Cu(1)–N(7)	93.04(8)/93.46(11)	N(10)–Cu(1)–N(4)	171.53(8)/172.04(12)
N(4)–Cu(1)–N(7)	78.50(8)/78.65(11)	N(10)–Cu(1)–N(1)	93.55(8)/92.92(11)
N(7)–Cu(1)–N(1)	166.68(9)/167.51(11)	N(4)–Cu(1)–N(1)	94.63(8)/94.64(11)
$N(4)^{\#1}$–Cu(2)–N(4)	180.0/180.0	$N(4)^{\#1}$–Cu(2)–N(7)	100.67(8)/100.77(11)
N(4)–Cu(2)–N(7)	79.33(8)/79.23(11)	$N(7)^{\#1}$–Cu(2)–N(7)	180.0/180.0

Symmetry transformations used to generate equivalent atoms: #1 $-x, -y + 1, -z$.

 This journal is © The Royal Society of Chemistry 2010

Downloaded by University of Chicago on 22/04/2013 15:54:28.
Published on 09 July 2010 on http://pubs.rsc.org | doi:10.1039/C0DT00181C

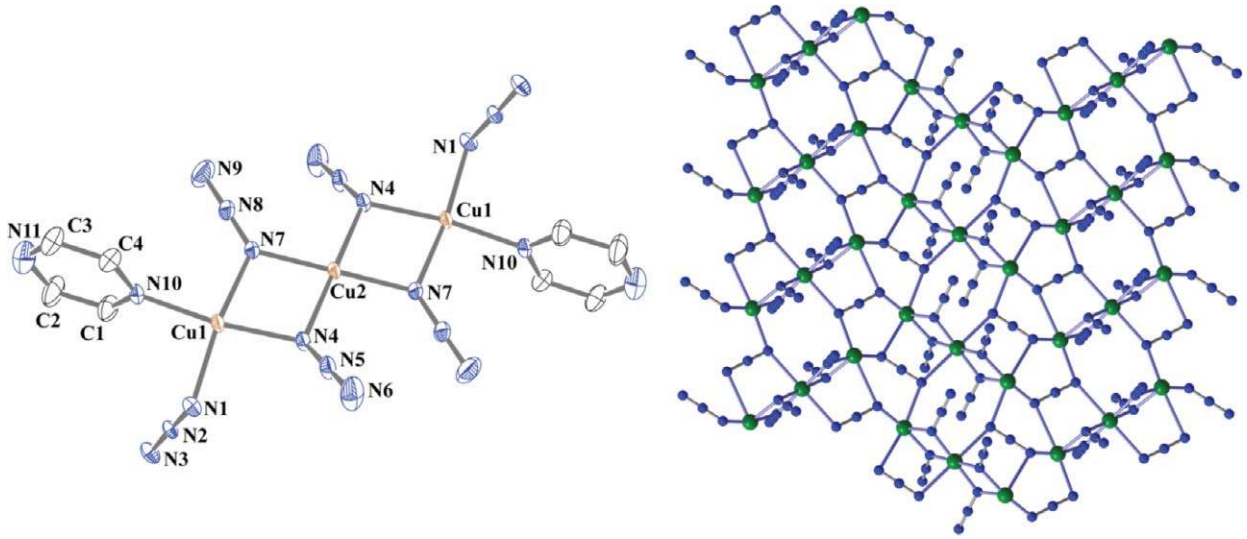

Fig. 5 ORTEP view of the basic unit (left) and the 2D network (right, pyz ligands omitted for clarity) as viewed perpendicular to the crystallographic *bc* plane of **4**. Hydrogen atoms have been removed for clarity. Thermal ellipsoids are at 30% probability level.

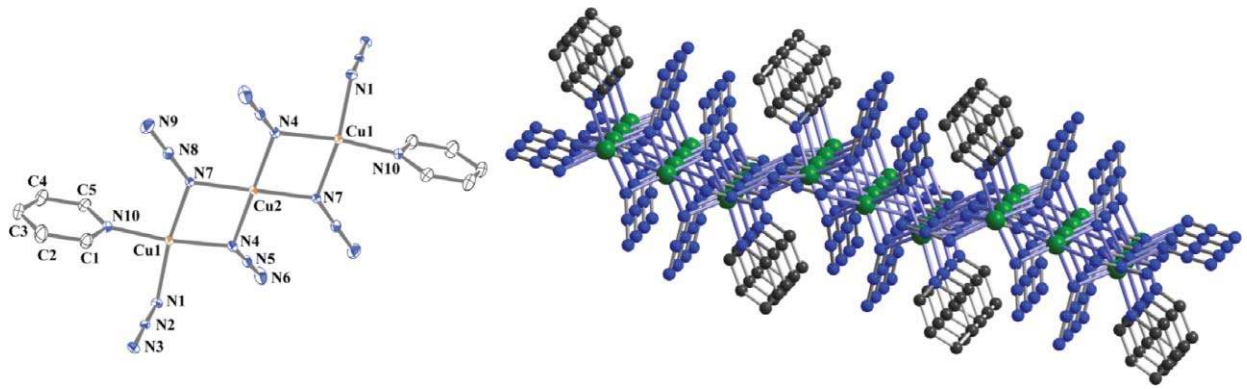

Fig. 6 ORTEP view of the basic unit (left) and the 2D network (right) as viewed perpendicular to the crystallographic *ac* plane of **5**. Hydrogen atoms have been removed for clarity. Thermal ellipsoids are at 30% probability level.

and $[Cu_3(N_3)_6L_2]$[34] [where Meinic = methylisonicotinate, ampym = 2-aminopyrimidine, and L = hydridotris(3,5-dimethylpyrazolyl)borate] have a symmetric trinuclear unit (just like **4** and **5**); $[Cu_3(N_3)_6(det)_2]$[35] has an asymmetric unit and another two complexes $[Cu_3(N_3)_6(2,2\text{-tpcb})(DMF)_2]_n$[36] and $[Cu_3(N_3)_6(tmen)_2]_n$[37] have irregular trinuclear asymmetric units. All of these six complexes are either discrete or 1D in nature, but **4** and **5** are the first 2D complexes in this series.

Magnetic behavior

Complex 1. Fig. 7 shows the dc magnetic susceptibility data measured on a polycrystalline powdered sample of **1** under an applied field of 500 G as both χ_M *vs.* T and $\chi_M T$ *vs.* T plots (where χ_M is the molar magnetic susceptibility per Co^{II}_2 unit). The room temperature (300 K) $\chi_M T$ value of 6.62 cm^3 K mol^{-1} is within the normal range for two uncoupled octahedral Co^{II} with an unquenched orbital momentum. As the temperature is lowered, the $\chi_M T$ value first decreases smoothly to a minimum at about 54 K ($\chi_M T = 5.08$ cm^3 K mol^{-1}), then rises rapidly to a sharp maximum at 14 K ($\chi_M T = 7.22$ cm^3 K mol^{-1}), and eventually drops rapidly due to saturation effects ($\chi_M T = 1.87$ cm^3 K mol^{-1} at 2 K).

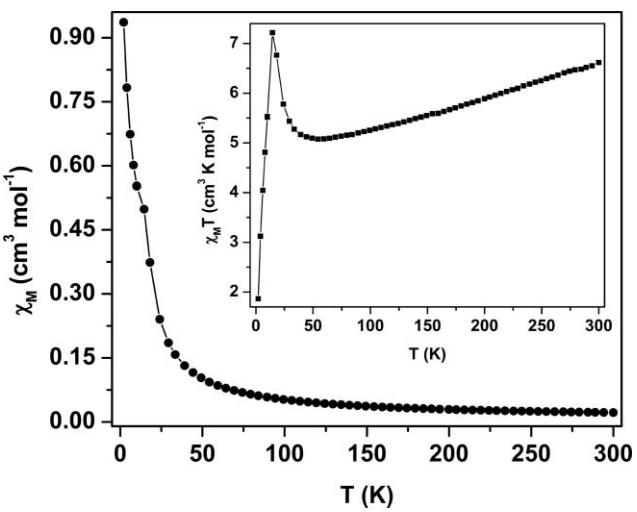

Fig. 7 Plots of χ_M *vs.* T and $\chi_M T$ *vs.* T (inset) for complex **1** in the temperature range of 2–300 K (solid lines are a guide for the eye).

The $1/\chi_M$ *vs.* T plot above 70 K followed the Curie–Weiss law with $\theta = -44.36$ K. The initial decrease of $\chi_M T$ and the

Downloaded by University of Chicago on 22/04/2013 15:54:28.
Published on 09 July 2010 on http://pubs.rsc.org | doi:10.1039/C0DT00181C

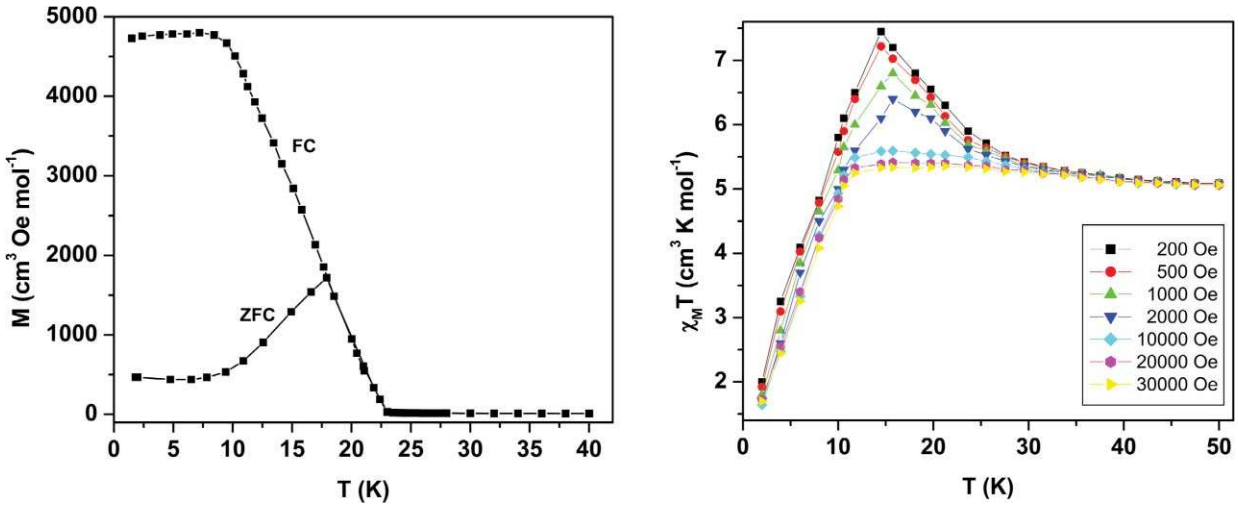

Fig. 8 Plots of the FC and ZFC magnetization (left) and the field dependent $\chi_M T$ *vs.* T plots for complex **1** (right) in the temperature range of 2–50 K (solid lines are guide for the eye).

significantly large negative Weiss constant (θ) could be a result of the simultaneous operation of the ligand field effects, spin–orbit coupling of Co^{II} ions and/or, the antiferromagnetic interaction along the chain associated with the weak ferromagnetic interaction between the Co^{II} ions through azido bridges in the dimeric unit or significant orbital contribution. On the other hand, the steep rises in both χ_M and $\chi_M T$ values at low temperature indicate that a kind of spontaneous magnetization sets on. In this kind of "canted antiferromagnetism" the antiferromagnetically coupled spins from different sublattices are not perfectly antiparallel, but are canted to each other. It results in the correlation of the net moments in a ferromagnetic-like fashion and builds up into long-range ordering below the critical temperature.

To illustrate the low temperature behavior of **1**, FC (field-cooled) and ZFC (zero-field-cooled) magnetization measurements were performed (Fig. 8). The lower temperature FC-susceptibilities are strongly dependent upon the applied field, as expected for spin canted systems (Fig. 8). The FC-magnetization (for all fields measured), increases rapidly below 30 K and approaches the saturation value below 20 K, which indicates that the field-cooling procedure creates a weak ferromagnetic state in which the spin-canted antiferromagnetic layers are ferromagnetically ordered. The critical temperature was estimated to be, $T_C = 18.0$ K, at which the FC dM/dT derivative curve shows a sharp minima. The T_C value was also confirmed by the observation that the FC and ZFC curves merge at 18 K (Fig. 8).

To further characterize the weak ferromagnetism at low temperature in **1**, the isothermal field dependence magnetization experiment was performed at 2 K (Fig. 9). The initial magnetization plot indicates that magnetization first increases reasonably fast up to about 0.5 T, but upon a further increase of the field, the magnetization increases much more slowly as the ferromagnetic phase tends to saturate (Fig. 9). Finally, the magnetization increases almost linearly for the higher fields, which is a feature of spin-canting antiferromagnet.

At 2 K complex **1** exhibits a hysteresis loop, related to the anisotropy of Co^{II}. It behaves as a soft magnet with a coercive field of 3.2 kOe and a remnant magnetization of 0.16 Nβ. The spontaneous magnetization is presumably due to spin canting, which

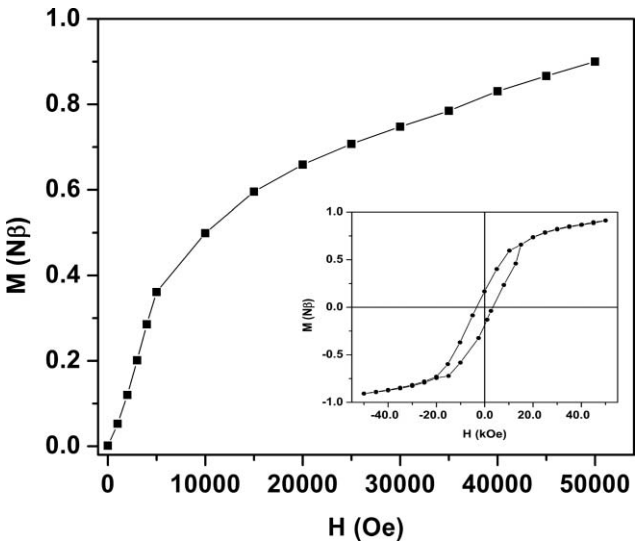

Fig. 9 Plot of M *vs.* H at 2 K for **1**. The inset shows hysteresis loop at 2 K.

was further supported by the fact that the saturated magnetization value at 5 T is considerably lower than the theoretical saturation value. The estimated canting angle of 3.05° was obtained from the equation $\psi = \sin^{-1}(M_r/M_s)$[38] where M_r is remnant magnetization (0.16 Nβ) and M_s ($M_s = gS = 3$ in the present case) is the expected saturated magnetization if all the moments are aligned ferromagnetically.

Complex 2. The dc magnetic susceptibility measured on a powder sample of **2** under an applied field of 1000 G is shown in Fig. 10 as both χ_M *vs.* T and $\chi_M T$ *vs.* T plots (where χ_M is the molar magnetic susceptibility per Mn^{II} unit). At room temperature (300 K) $\chi_M T$ value is 4.75 cm^3 K mol^{-1}, and it gradually increases upon lowering the temperature, with a sharp jump below 50 K and reaches a maximum value of 7.56 cm^3 K mol^{-1} at 10 K and finally decreases to 5.60 cm^3 K mol^{-1} at 2 K. The $1/\chi_M$ *vs.* T plots (300–20 K) obey the Curie–Weiss law with a positive Weiss constant of $\theta = 10.71$ K indicating a dominant ferromagnetic exchange

 This journal is © The Royal Society of Chemistry 2010

Published on 09 July 2010 on http://pubs.rsc.org | doi:10.1039/C0DT00181C
Downloaded by University of Chicago on 22/04/2013 15:54:28.

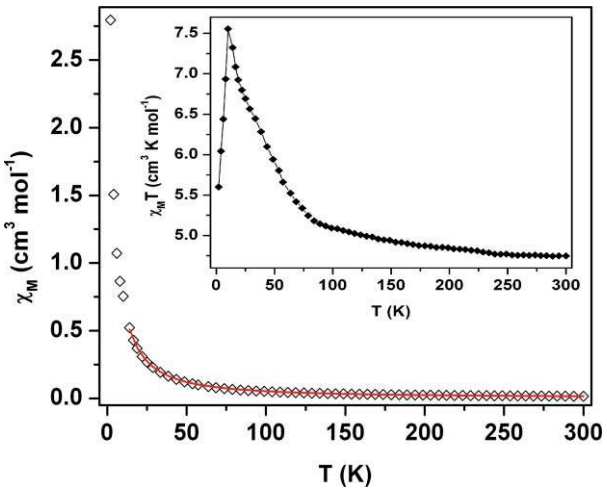

Fig. 10 Plots of χ_M *vs.* T and $\chi_M T$ *vs.* T (inset) for complex **2** in the temperature range of 2–300 K. The red line indicates the fitting using theoretical model (see text).

between the neighboring Mn^{II} ions. The only exchange pathway is through the double EO-azido bridges (J). A reasonable fit was obtained for interacting dinuclear units applying the conventional Hamiltonian:

$$H = -JS_1S_2 \text{ where } S_1 = S_2 = 5/2$$

modified by introducing an interdimer zJ' term. Considering these two different exchange parameters, the analysis of the experimental susceptibility values has been performed with the best fit values as follows: $J = 2.75$ cm^{-1} and $zJ' = -0.03$ cm^{-1} for $g = 2$ ($R = 5.25 \times 10^{-5}$).

Complex 3. Fig. 11 shows the dc magnetic susceptibility measured on a powder sample of **3** under an applied field of 1000 G as both χ_M *vs.* T and $\chi_M T$ *vs.* T plots (where χ_M is the molar magnetic susceptibility per Mn^{II} unit). The room temperature (300 K) $\chi_M T$ value (3.67 cm^3 K mol^{-1}) is significantly lower than that expected for an uncoupled Mn^{II} ion which is indicative of the

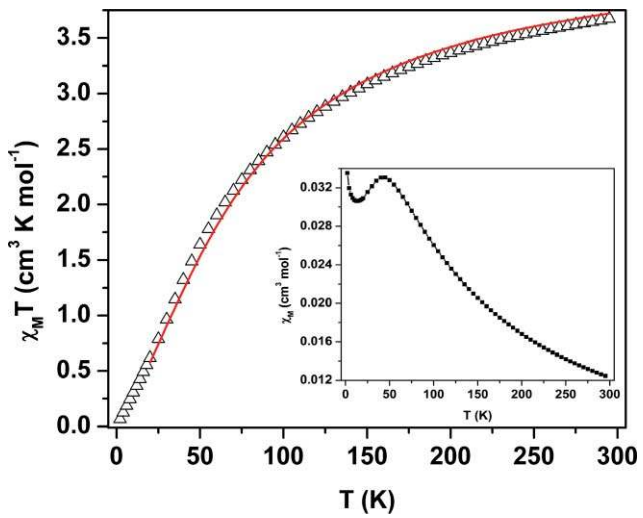

Fig. 11 Plots of $\chi_M T$ *vs.* T and χ_M *vs.* T (inset) for complex **3** in the temperature range of 2–300 K. The red line indicates the fitting using Fischer's model (see text).

presence of antiferromagnetic exchange between the metal ions. The $\chi_M T$ value gradually decreases with decreasing temperature but a sharp decrease is visible below 75 K, and reaches 0.07 cm^3 K mol^{-1} at 2 K. The $1/\chi_M$ *vs.* T plot (300–50 K) obey the Curie–Weiss law with a negative Weiss constant of $\theta = -84.59$ K indicating a dominant antiferromagnetic exchange between the neighboring Mn^{II} ions.

The 2D complex consists of magnetically uniform Mn^{II} chains linked by azido and carboxylate superexchange pathways. A reasonable fit could be obtained with the well known Fischer's[39a] model for infinite chains of classical spins for temperatures above 20 K using the expression:

$$\chi_{chain} = [Ng^2\beta^2S(S+1)/3kT][(1+u)/(1-u)]$$

where, $u = coth[JS(S+1)/kT] - kT/JS(S+1)$ *and* $S = 5/2$.

The exchange parameter J is based on the Hamiltonian $H = -2J\sum S_iS_{i+1}$ and the operator S is treated as a classical spin operator. The inter-chain interaction (zJ') can be treated by the molecular field approximation:[39b]

$$X_{inter} = \chi_{chain}/\{1 - \chi_{chain}(2zJ'/Ng^2\beta^2)\}.$$

The best fit parameters thus obtained are $J = -4.02$ cm^{-1}, $zJ' = -0.03$ cm^{-1} for $g = 2$ with the agreement factor $R = 1.32 \times 10^{-4}$.

A better fit was obtained for an interacting dimer model above 12 K applying the conventional Hamiltonian:

$$H = -JS_1S_2 \text{ where } S_1 = S_2 = 5/2$$

modified by introducing an interdimer zJ' term. The analysis resulted in the best fit values as $J = -4.95$ cm^{-1} and $zJ' = -0.01$ cm^{-1} for $g = 2$ ($R = 1.22 \times 10^{-5}$).

Complexes 4 and 5. Fig. 12 shows the temperature dependence of χ_M and $\chi_M T$ values for complexes **4** and **5**. The similarities of these two complexes in structure are clearly reflected in their magnetic properties also. At room temperature $\chi_M T = 1.39$ cm^3 K mol^{-1} for **4** and 1.40 cm^3 K mol^{-1} for **5** ($\chi_M T = 0.375$ cm^3 K mol^{-1} for an $S = 1/2$ ion), both the values being a little higher than expected for three uncoupled Cu^{II} ions. The $\chi_M T$ value gradually increases upon decreasing the temperature from 300 K and reaches a maximum value of 1.78 cm^3 K mol^{-1} at 37 K for **4** and 1.80 cm^3 K mol^{-1} at 35 K for **5**. Further cooling decreases the $\chi_M T$ value to 0.82 cm^3 K mol^{-1} and to 0.85 cm^3 K mol^{-1} at 2 K for **4** and **5** respectively. The $1/\chi_M$ *vs.* T plots (300–25 K) obey the Curie–Weiss law with a positive Weiss constants of $\theta = 18.89$ K (**4**) and 19.31 K (**5**). The nature of the $\chi_M T$ *versus* T plots and the positive θ suggest a dominant ferromagnetic exchange among the three Cu^{II} ions through azido bridges for both the complexes.

From the structural point of view for these two centrosymmetric complexes, the two EO-azido bridges between Cu(2) and two Cu(1) ion on both sides account for the magnetic exchange pathway. Symmetry makes the two exchange parameters (J) to be the same. A reasonable fit can be obtained for interacting trinuclear units applying the conventional Hamiltonian:

$$H = -J(S_1S_2 + S_2S_3)$$

modified by introducing an intertrimer zJ' term. Considering these two different exchange parameters, the analysis of the

Published on 09 July 2010 on http://pubs.rsc.org | doi:10.1039/C0DT00181C
Downloaded by University of Chicago on 22/04/2013 15:54:28.

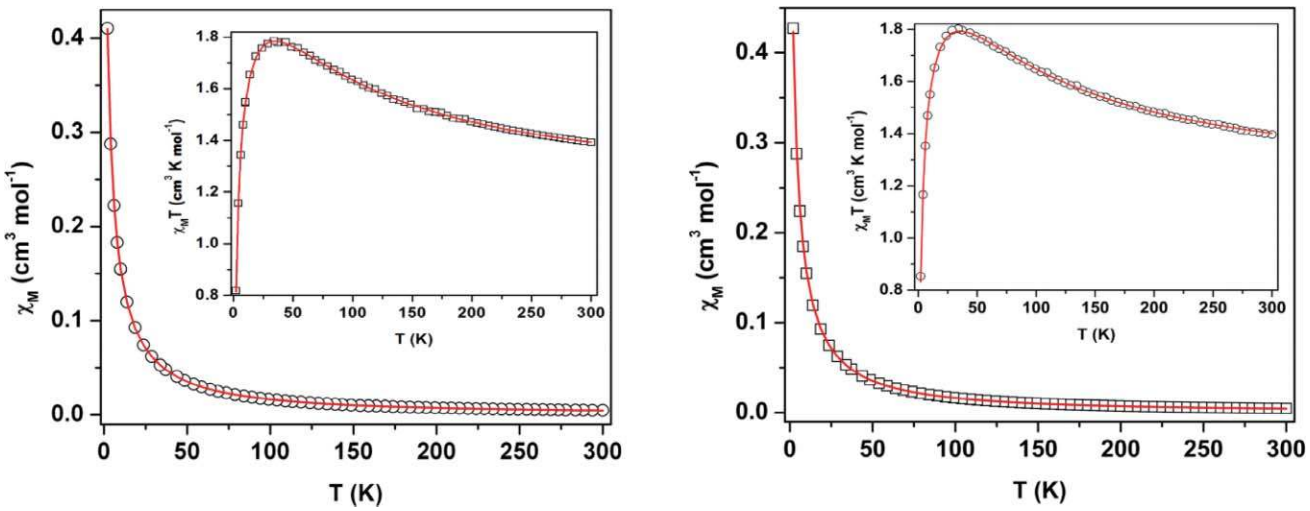

Fig. 12 Plots of χ_M *vs.* T and $\chi_M T$ *vs.* T (inset) for complex **4** (left) and **5** (right) in the temperature range of 2–300 K. The red lines indicate the fitting using theoretical model (see text).

Table 4 Best-fit values of magnetic exchange parameters for **4** and **5**

Complex	J/cm^{-1}	zJ'/cm^{-1}	g	R
4	118.76	–0.81	2.06	1.73×10^{-5}
5	125.48	–0.78	2.06	2.54×10^{-5}

experimental susceptibility values has been performed using the following expression:

$$\chi_M = \chi_M'/\{1 - \chi_M'(2zJ'/Ng^2\beta^2)\}$$

$$\chi_M' = (Ng^2\beta^2/3kT)[A/B]$$

where $A = [15\exp(3J/2kT) + (3/2)\exp(J/kT) + (3/2)]$ and $B = [4\exp(3J/2kT) + 2\exp(J/kT) + 2]$ and the best fit values for the two complexes have been shown in Table 4.

Theoretical study

To understand the magnetic behavior and gain some insight into the exchange mechanism of all the five complexes, quantum mechanical density functional theory (DFT) calculations were performed with the *Gaussian 03* package using B3LYP functional and employing LANL2DZ as a basis with broken symmetry formalism (BS). In all the cases our main aim corresponds to the exploration of the coupling interaction between the paramagnetic centers through the bridging ligands.

It is a common practice in the field of polymeric metal complexes to compute the exchange interactions using a model structure that very nearly resembles the repeating unit of the particular complex, mainly to reduce the computational time. We have taken dinuclear units for the complexes **1**, **2** and **3**, and trinuclear units for the complexes **4** and **5** with small modifications for the computational simplification as the model structures (Fig. 13). Such modifications are generally adopted in these calculations and expected not to introduce significant errors. Ligand modification is very common in the calculation of magnetic property of transition metal polymeric complexes for accelerating SCF (self consistent field) convergence.[40] It has been shown, however, that this modifications can have an important effect on the absolute value of the exchange parameter J to be compared with the experiment, and therefore, only a qualitative agreement between experimental and computed data could be expected. Any other better result can be considered as fortuitous. The same computational methodology was used in all the cases, based on the following steps: (i) the geometry as obtained from the crystallographic data was optimized after modifications in their high spin states; (ii) the optimized geometry confirmed as in the global minima in the potential energy surface; and (iii) hence, single point calculations using broken symmetry approach were carried out for the different spin states of all the complexes.

On the basis of the relative energy of the high-spin and the low-spin states the magnetic coupling constant of the all complexes were calculated. A large number of studies using quantum calculations intended to determine the value of the coupling constant J, through the broken-symmetry (BS) approach, have been published.[41] The value of the coupling parameter J can be obtained[42] using the equation

$$J = \frac{({}^{DFT}E_{BS} - {}^{DFT}E_{HS})}{S^2_{max}}$$

where E_{HS} is the calculated energy for the highest spin states, E_{BS} is the energy of the lowest spin states obtained by broken symmetry approach and $S^2{}_{max} = 1 - S_{ab}{}^2$, S_{ab} being the overlap integral between centers a and b.

The extent of magnetic interaction is related to the amount of spin density transferred from one magnetic center to the other. In transition metal complexes the spin density is mostly concentrated on the metal center. The degree of spin density transfer to the ligand is an indication of how strong the magnetic interaction is. We defined the magnetic centers according to the spin distribution computed with the Mulliken population analysis (Mulliken's spin populations) for the broken symmetry wave function in all the cases.

For complex **1** (with three unpaired electrons on each cobalt atom, Scheme 1), J value was calculated considering the difference

 This journal is © The Royal Society of Chemistry 2010

Downloaded by University of Chicago on 22/04/2013 15:54:28.
Published on 09 July 2010 on http://pubs.rsc.org | doi:10.1039/C0DT00181C

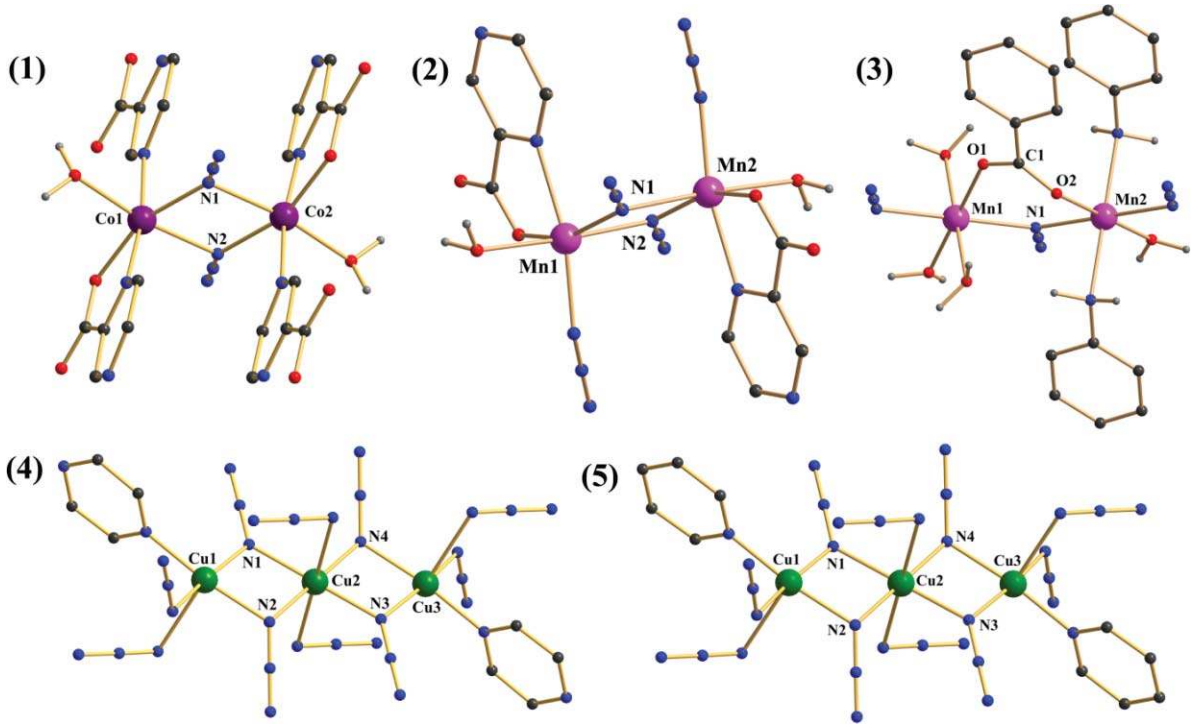

Fig. 13 Model complexes for the DFT calculation (as derived from the crystal structures).

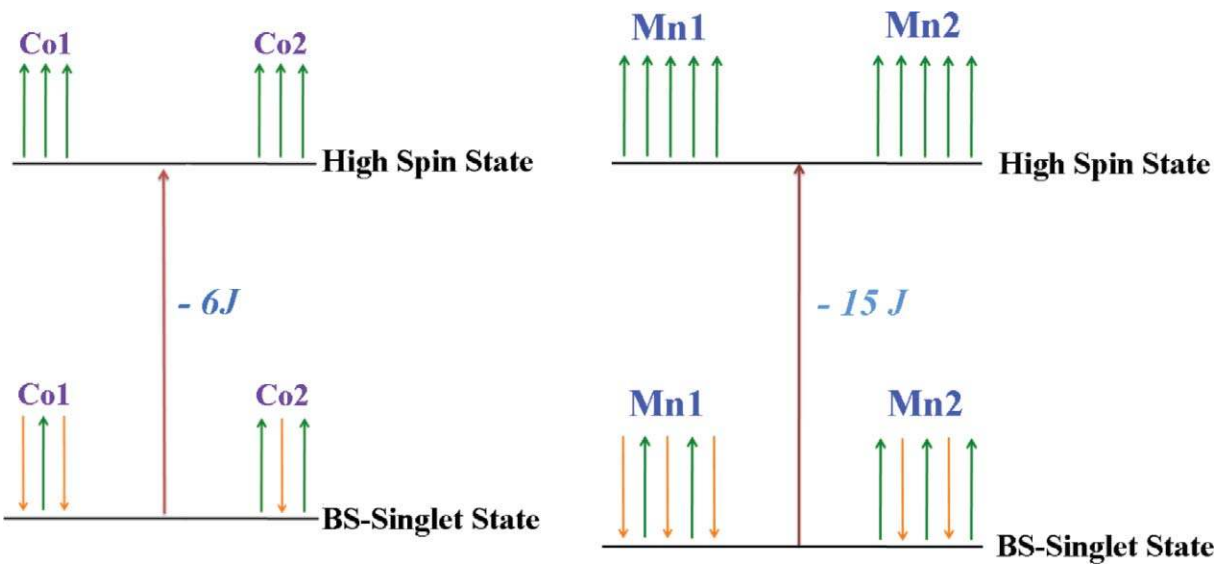

Scheme 1 Energy difference between the highest spin and broken symmetry states for **1** (left) and for **2** and **3** (right).

in energy (−6*J*) between the high-spin state (multiplicity 7) and the broken symmetry low-spin state (singlet). Magnetic exchange through double EO-azido bridges with both the Co–N–Co angle 103.68° is expected to be moderately strong ferromagnetic in nature. The calculated *J* of 184.6 cm^{-1} is in well agreement to this expectation. Though we were unable to fit the experimental data, the initially decreasing $\chi_M T$ value clearly indicates that the overall magnetic behavior of this complex is much more intricate in nature and the canted antiferromagnetism observed has its origin to the overall structure of the complex.

The spin-density analysis (Fig. 14) reveals that these densities are very much concentrated on the Co^{II} ions and the two bridging nitrogen atoms of the azido groups. It is found that the spin populations on the paramagnetic metal atom and bridging nitrogen ligand are of the same sign in the high-spin (low energy) state. The spin density values are 2.6896 e^- and 2.6888 e^- for Co1 and Co2 respectively, whereas that in their low-spin state are –0.9619 e^- and 0.9745 e^-. This spin density distribution is the origin of the strong ferromagnetic coupling.

Complexes **2** and **3**, with five unpaired electrons residing on the each Mn^{II} ions correspond to the high spin state of multiplicity

Published on 09 July 2010 on http://pubs.rsc.org | doi:10.1039/C0DT00181C
Downloaded by University of Chicago on 22/04/2013 15:54:28.

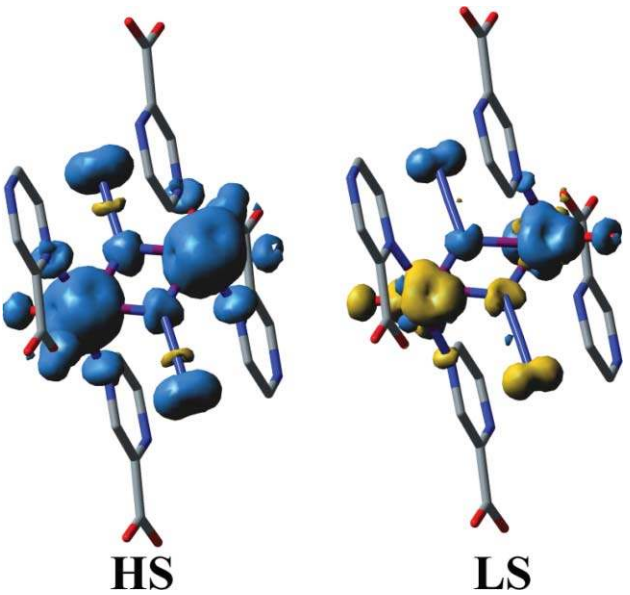

Fig. 14 Calculated spin density map for the complex **1** for high-spin state and broken symmetry singlet state. The blue surface corresponds to the positive spin density and yellow surface for negative one. The isodensity surface corresponds to the cut off value 0.003 e bohr^{-3}.

11 and with the lowest spin state of a BS-singlet state. The J value was calculated taking into account the difference of the energy of these two states (which equals to $-15J$). The DFT calculation of **2** predicts strong ferromagnetic interaction with $J = 81.6$ cm^{-1}, which is expected with two EO-azido bridge having both Mn–N–Mn angle 100.23°, with respect to the experimental very weak ferromagnetic nature of $J = 2.75$ cm^{-1}. However, the DFT calculation predicts very weak antiferromagnetic interaction for **3** with $J = -11.5$ cm^{-1}, which is in fairly good agreement with the experimental value of –4.95 cm^{-1}. It seems logical that the EO-azido bridge with Mn–N–Mn angle of 121.8° transmits antiferromagnetic interaction and furthermore, the carboxylato bridge in *syn–syn* coordination mode is also expected to contribute to the same.

The calculated spin density for the high-spin state and singlet state of **2** and **3** (Fig. 15) offers information on the electronic structure and the mechanism of the magnetic exchange interaction. The quasi spherical shape of the Mn^{II} atoms occur generally for a set of five d orbitals with one unpaired electron on each.[43] The sphere is somewhat flattened in the directions of the metal–ligand bonds and small spin densities of the same sign appear on the atoms of the ligands directly attached to the metallic centre in high spin state. This loss of sphericity at the Mn^{II} atoms is the result of the lesser spin density at the e_g orbitals than at the t_{2g} orbitals, which is a consequence of the significant spin density delocalization for the σ-type e_g orbitals to the donor atoms of the ligands. Actually, the whole spin density is primarily located on the metallic centers (average value of 4.58 e$^-$ for **2** and 4.79 e$^-$ for **3**) in the high spin state. For **3** the bridging nitrogen of azide have a spin density of –0.0388 e$^-$ and an average of 0.025 e$^-$ on the two oxygen atoms, 0.002 e$^-$ on the carbon atom of carboxylate group respectively; suggesting that the delocalization process does not significantly operate in this case. This is in agreement with the weak magnetic coupling observed. The lower spin density on Mn^{II} in **2** with respect

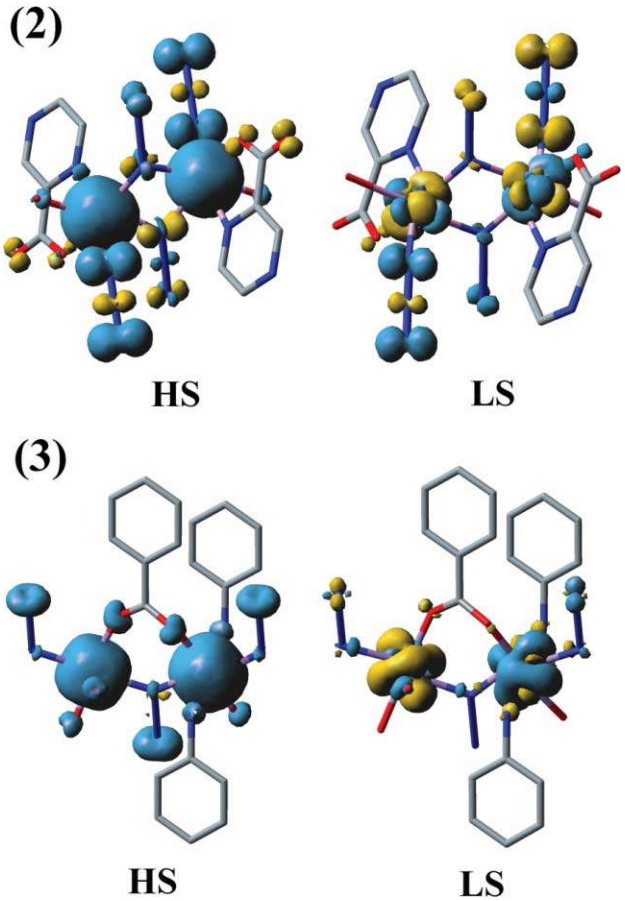

Fig. 15 Calculated spin density map for the complex **2** and **3** for high spin state and broken symmetry singlet state. The blue surface corresponds to the positive spin density and yellow surface for negative one. The isodensity surface corresponds to the cut off value 0.005 e bohr^{-3}.

to that in **3** indicates strong interaction between two manganese centres in the former. Small spin densities of the same sign appear on the atoms of the ligands directly attached to the metallic centre in **3** but not in **2**, where the bridging N atom has different spin density. Interestingly, in the low spin state of these two complexes the spin density on Mn1 and Mn2 are 0.3068 e$^-$ and –0.3066 e$^-$ in **2**, and that in **3** are 1.035 e$^-$ and –1.025 e$^-$ respectively.

In the case of the Cu complexes **4** and **5**, the J values were calculated from their intrinsic energy difference between the quartet state and the corresponding broken symmetry doublet state. The DFT calculated $J = 147.8$ cm^{-1} and 213.6 cm^{-1} for **4** and **5** respectively corresponds to strong ferromagnetic coupling and are in reasonably good agreement with the experimentally calculated values of 118.76 cm^{-1} and 125.48 cm^{-1}. It is reasonable to expect strong ferromagnetic exchange between the Cu^{II} ions as all the coupling interactions are through the equatorial plane and all the Cu–N–Cu bridging angles are around 100.5°.

Mulliken spin density analysis for all the states of both the complexes also reveals how the strong ferromagnetic interaction between the Cu centers actually operates. The spin density map for all the states are given in the Fig. 16. It is observed that most of the spin density is concentrated on the Cu^{II} ions and the bridging nitrogen atoms. In the high spin states the spin density at each Cu atom of **4** and **5** has the shape of a $d_{x^2-y^2}$ orbital and it is

 This journal is © The Royal Society of Chemistry 2010

Published on 09 July 2010 on http://pubs.rsc.org | doi:10.1039/C0DT00181C
Downloaded by University of Chicago on 22/04/2013 15:54:28.

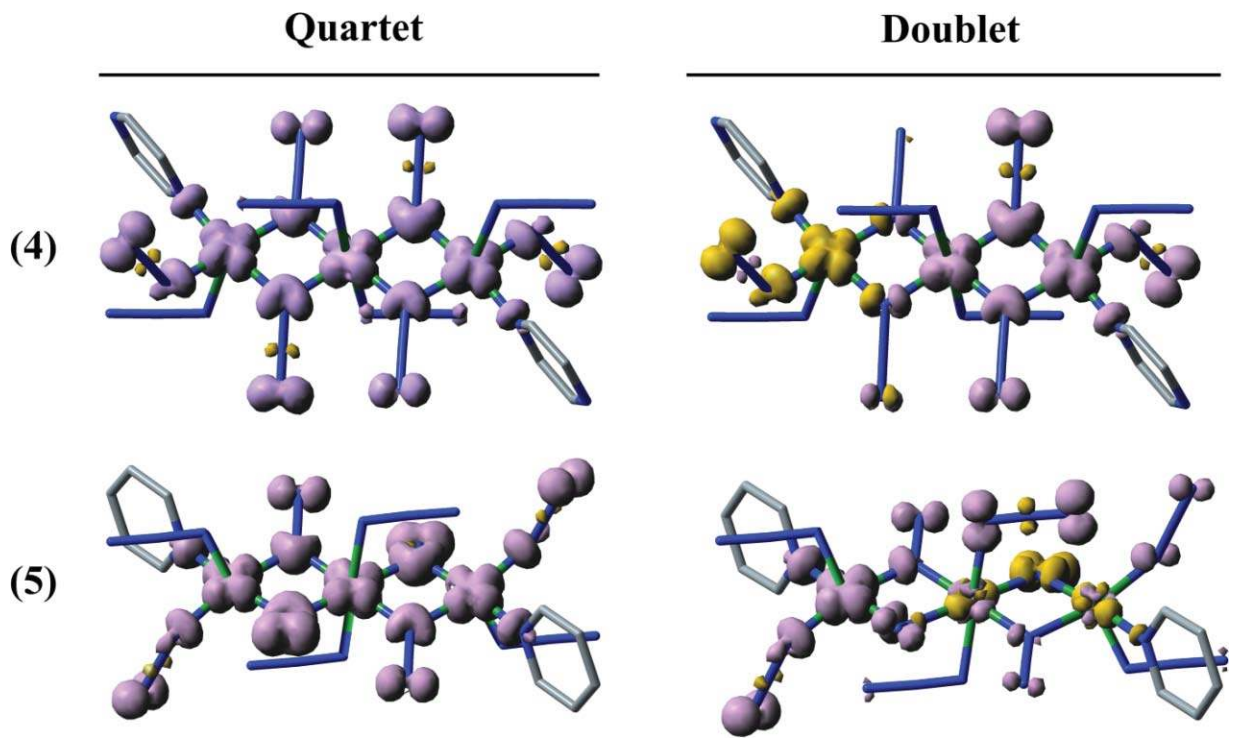

Fig. 16 Calculated spin density map for the complex **4** and **5** for high spin and broken symmetry doublet states. The violet surface corresponds to the positive spin density and yellow surface for the negative one. The isodensity surface corresponds to the cut off value of 0.003 e bohr^{-3}.

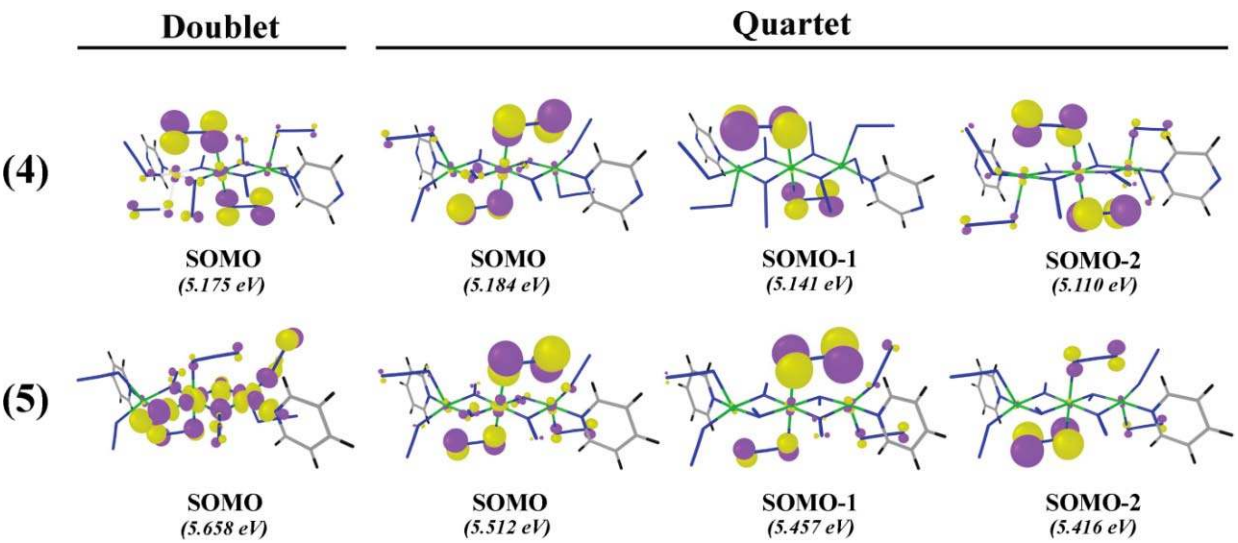

Fig. 17 SOMOs for compound **4** and **5**, yellow and violet colors represent positive and negative electronic density. The isodensity surface corresponds to 0.035 e bohr^{-3}.

delocalized on the bridging atoms, which also carry positive spin densities. The spin density value of the Cu^{II} atoms and the bridging atoms of both the complexes are given in Table S2 (ESI†).

Magnetic orbital analysis is often used to explore the trail of magnetic coupling in magnetic molecules. The singly occupied molecular orbitals (SOMO) are given in Fig. 17 for both the complexes. It is clear from the SOMOs of **4** and **5**, that, as expected, the exchange pathway is of the σ type, involving the $d_{x^2-y^2}$ magnetic orbitals of the Cu atoms and the sp^2 hybrid orbitals of the bridging nitrogen atoms. Moreover, SOMOs show that the atomic orbitals with a higher contribution to these molecular orbitals are those of the non-bridging nitrogen atoms.

Concluding remarks

We have demonstrated how the powerful solvothermal technique offers new opportunities in the synthesis of polynuclear transition metal complexes using simple bridging ligands. When we combined other anionic and neutral ligands with the very familiar azido ligand, we could isolate five new coordination polymeric

Published on 09 July 2010 on http://pubs.rsc.org | doi:10.1039/C0DT00181C
Downloaded by University of Chicago on 22/04/2013 15:54:28.

architectures that differ significantly in their structure and magnetic properties. With pyrazine-2-carboxylate (pyzc) we obtained a 1D cobalt complex **1**, which exhibits canted antiferromagnetic behavior, while the heterometallic 3D complex **2** is simply ferromagnetic in nature. Complex **3** was synthesized changing the carboxylate ligand to *p*-aminobenzoate and this 2D polymer was found to be antiferromagnetic in nature. An unexpected decarboxylation of the ligand pyzc under vigorous reaction conditions afforded a new Cu-azido complex with a neutral donor pyrazine (**4**), which was followed by the isolation of an isostructural complex with the neutral donor ligand pyridine (**5**). These two ferromagnetic complexes exhibit almost identical variable temperature magnetic behavior. We also investigated the magnetic properties through some theoretical calculations (DFT) using suitably modeled structures derived directly from the crystal structures that revealed the underlying mechanism of magnetic exchange and predicted the exchange constants with a fair degree of accuracy.

The findings in this work offer crucial information for the design of molecular magnetic materials, and demonstrate the potentials and difficulties of controlling bulk magnetic properties at the supramolecular level. Studies along this line may also help to further uncover the magnetic intricacy and miscellany in molecular systems.

Acknowledgements

Authors thank the Department of Science and Technology (DST), New Delhi for financial support. S. M. gratefully acknowledges the Council of Scientific and Industrial Research, New Delhi, India for the award of a Research Fellowship. Authors sincerely thank Prof. Mike Drew for his kind help on the structure determination of complex **1**.

References

1 (*a*) R. E. P. Winpenny, *Angew. Chem., Int. Ed.*, 2008, **47**, 7992; (*b*) N. L. Toh, M. Nagarathinam and J. J. Vittal, *Angew. Chem., Int. Ed.*, 2005, **44**, 2167; (*c*) M. C. Das and P. K. Bharadwaj, *J. Am. Chem. Soc.*, 2009, **131**, 10942; (*d*) M. Eddaoudi, J. Kim, N. Rosi, D. Vodak, J. Wachter, M. O'Keeffe and O. M. Yaghi, *Science*, 2002, **295**, 469; (*e*) P. Lama, A. Aijaz, E. C. Sanudo and P. K. Bharadwaj, *Cryst. Growth Des.*, 2010, **10**, 283; (*f*) D. N. Dybtseb, H. Chun, S. H. Yoon, D. Kim and K. Kim, *J. Am. Chem. Soc.*, 2004, **126**, 32; (*g*) D. Moon, S. Kang, J. Park, K. Lee, R. P. John, H. Won, Y. S. Kim, G. H. Kim, H. Rhee and M. S. Lah, *J. Am. Chem. Soc.*, 2006, **128**, 3530; (*h*) M. J. Prakash, M. Oh, X. Liu, K. N. Han, G. H. Seong and M. S. Lah, *Chem. Commun.*, 2010, **46**, 2049; (*i*) M. Bannerjee, S. Das, M. Yoon, H. J. Choi, M. H. Hyun, S. M. Park, G. Seo and K. Kim, *J. Am. Chem. Soc.*, 2009, **131**, 7524.

2 (*a*) L. Carlucci, G. Ciani and D. M. Proserpio, *Coord. Chem. Rev.*, 2003, **246**, 247; (*b*) S. Das, H. Kim and K. Kim, *J. Am. Chem. Soc.*, 2009, **131**, 3814; (*c*) A. M. P. Peedikakkal and J. J. Vittal, *Inorg. Chem.*, 2010, **49**, 10; (*d*) W. Ouellette, J. R. Galan-Mascaros, K. R. Dunbar and J. Jubieta, *Inorg. Chem.*, 2006, **45**, 1909; (*e*) S. Supriya and S. K. Das, *J. Am. Chem. Soc.*, 2007, **129**, 3464.

3 (*a*) S. Kitagawa, R. Kitaura and S. Noro, *Angew. Chem., Int. Ed.*, 2004, **43**, 2334; (*b*) S. Kitagawa and K. Uemura, *Chem. Soc. Rev.*, 2005, **34**, 109.

4 (*a*) H. R. Zhao, D. P. Li, X. M. Ren, Y. Song and Q. W. Jin, *J. Am. Chem. Soc.*, 2010, **132**, 18; (*b*) O. Kahn, *Molecular Magnetism*, VCH, New York, 1993; (*c*) J. S. Miller, *Adv. Mater.*, 2002, **14**, 1105; (*d*) *Magnetism: Molecules to Materials, Vol.* I–V (ed. J. S. Miller and M. Drillon), Wiley-VCH, Weinheim, 2002–2005; (*e*) Special issue on Magnetism - Molecular, Supramolecular Perspectives, *Coord. Chem. Rev.*, 2005, 249.

5 (*a*) D. Gatteschi and R. Sessoli, *Angew. Chem., Int. Ed.*, 2003, **42**, 268; (*b*) C. Coulon, H. Miyasaka and R. Clérac, *Struct. Bonding*, 2006, **122**, 163.

6 (*a*) S. M. Humphrey and P. T. Wood, *J. Am. Chem. Soc.*, 2004, **126**, 13236; (*b*) W.-K. Chang, R.-K. Chiang, Y.-C. Jiang, S.-L. Wang, S.-F. Lee and K.-H. Lii, *Inorg. Chem.*, 2004, **43**, 2564; (*c*) E. Colacio, J. M. Domínguez-Vera, M. Ghazi, R. Kivekäs, F. Lloret, J. M. Moreno and H. Stoeckli-Evans, *Chem. Commun.*, 1999, 987.

7 (*a*) O. Sato, J. Tao and Y.-Z. Zhang, *Angew. Chem., Int. Ed.*, 2007, **46**, 2152; (*b*) E. Coronado and P. Day, *Chem. Rev.*, 2004, **104**, 5419; (*c*) D. R. Talham, *Chem. Rev.*, 2004, **104**, 5479; (*d*) D. Maspoch, D. Ruiz-Molina, K. Wurst, N. Domingo, M. Cavallini, F. Biscarini, J. Tejada, C. Rovira and J. Veciana, *Nat. Mater.*, 2003, **2**, 190; (*e*) E.-Q. Gao, S.-Q. Bai, Z.-M. Wang and C.-H. Yan, *J. Am. Chem. Soc.*, 2003, **125**, 4984.

8 (*a*) J. Ribas, A. Escuer, M. Monfort, R. Vicente, R. Cortés, L. Lezama and T. Rojo, *Coord. Chem. Rev.*, 1999, **193–195**, 1027; (*b*) X.-Y. Wang, Z.-M. Wang and S. Gao, *Chem. Commun.*, 2008, 281; (*c*) E.-Q. Gao, Y.-F. Yue, S.-Q. Bai, Z. He and C.-H. Yan, *J. Am. Chem. Soc.*, 2004, **126**, 1419; (*d*) T.-F. Liu, D. Fu, S. Gao, Y.-Z. Zhang, H.-L. Sun, G. Su and Y.-J. Liu, *J. Am. Chem. Soc.*, 2003, **125**, 13976; (*e*) Y.-F. Zeng, J.-P. Zhao, B.-W. Hu, X. Hu, F.-C. Liu, J. Ribas, J. Ribas-AriÇo and X.-H. Bu, *Chem.–Eur. J.*, 2007, **13**, 9924; (*f*) B. Sarkar, S. Konar, C. J. Garcia and A. Ghosh, *Inorg. Chem.*, 2008, **47**, 11611.

9 (*a*) M. Murugesu, M. Habrych, W. Wernsdorfer, K. A. Abboud and G. Christou, *J. Am. Chem. Soc.*, 2004, **126**, 4766; (*b*) T. C. Stamatatos, K. A. Abboud, W. Wernsdorfer and G. Christou, *Angew. Chem., Int. Ed.*, 2007, **46**, 884; (*c*) Y.-Z. Zhang, W. Wernsdorfer, F. Pan, Z.-M. Wang and S. Gao, *Chem. Commun.*, 2006, 3302; (*d*) C. I. Yang, W. Wernsdorfer, G. H. Lee and H. L. Tsai, *J. Am. Chem. Soc.*, 2007, **129**, 456.

10 (*a*) A. Escuer, R. Vicente, M. A. S. Goher and F. A. Mautner, *Inorg. Chem.*, 1996, **35**, 6386; (*b*) M. A. S. Goher, J. Cano, Y. Journaux, M. A. M. Abu-Youssef, F. A. Mautner, A. Escuer and R. Vicente, *Chem.–Eur. J.*, 2000, **6**, 778; (*c*) F. A. Mautner, R. Cortés, L. Lezama and T. Rojo, *Angew. Chem., Int. Ed. Engl.*, 1996, **35**, 78; (*d*) S. Han, J. L. Manson, J. Kim and J. S. Miller, *Inorg. Chem.*, 2000, **39**, 4182; (*e*) A.-H. Fu, X.-Y. Huang, J. Li, T. Yuen and C.-L. Lin, *Chem.–Eur. J.*, 2002, **8**, 2239.

11 (*a*) P.-P. Liu, A.-L. Cheng, N. Liu, W.-W. Sun and E.-Q. Gao, *Chem. Mater.*, 2007, **19**, 2724; (*b*) E.-Q. Gao, A.-L. Cheng, Y.-X. Xu, M.-Y. He and C.-H. Yan, *Inorg. Chem.*, 2005, **44**, 8822; (*c*) E.-Q. Gao, Z.-M. Wang and C.-H. Yan, *Chem. Commun.*, 2003, 1748; (*d*) X.-Y. Wang, L. Wang, Z.-M. Wang and S. Gao, *J. Am. Chem. Soc.*, 2006, **128**, 674.

12 (*a*) A. Escuer, R. Vicente, M. A. S. Goher, F. A. Mautner and M. A. M. Abu-Youssef, *Chem. Commun.*, 2002, 64; (*b*) B.-Q. Ma, H.-L. Sun, S. Gao and G. Su, *Chem. Mater.*, 2001, **13**, 1946; (*c*) A. Escuer, R. Vicente, F. A. Mautner and M. A. S. Goher, *Inorg. Chem.*, 1997, **36**, 1233; (*d*) H.-J. Chen, Z.-W. Mao, S. Gao and X.-M. Chen, *Chem. Commun.*, 2001, 2320; (*e*) K. C. Mondal, O. Sengupta, M. Nethaji and P. S. Mukherjee, *Dalton Trans.*, 2008, 767; (*f*) O. Sengupta, R. Chakraborty and P. S. Mukherjee, *Dalton Trans.*, 2007, 4514.

13 (*a*) E.-Q. Gao, Y.-F. Yue, S.-Q. Bai, Z. He, S.-W. Zhang and C. H. Yan, *Chem. Mater.*, 2004, **16**, 1590; (*b*) A. Escuer, J. Cano, M. A. S. Goher, Y. Journaux, F. Lloret, F. A. Mautner and R. Vicente, *Inorg. Chem.*, 2000, **39**, 4688; (*c*) X.-Y. Wang, L. Wang, Z.-M. Wang, G. Su and S. Gao, *Chem. Mater.*, 2005, **17**, 6369; (*d*) A. Escuer, F. A. Mautner, M. A. S. Goher, M. A. M. Abu-Youssef and R. Vicente, *Chem. Commun.*, 2005, 605; (*e*) M. A. S. Goher, M. A. M. Abu-Youssef, F. A. Mautner, J. R. Vicente and A. Escuer, *Eur. J. Inorg. Chem.*, 2000, 1819; (*f*) B. Bitschnau, A. Egger, A. Escuer, F. A. Mautner, B. Sodin and R. Vicente, *Inorg. Chem.*, 2006, **45**, 868; (*g*) M. A. M. Abu-Youssef, V. Langer, D. Luneau, E. Shams, M. A. S. Goher and L. Öhrström, *Eur. J. Inorg. Chem.*, 2008, 112; (*h*) X.-T. Wang, Z.-M. Wang and S. Gao, *Inorg. Chem.*, 2007, **46**, 10452.

14 (*a*) M. A. M. Abu-Youssef, F. A. Mautner and R. Vicente, *Inorg. Chem.*, 2007, **46**, 4654; (*b*) X.-Y. Wang, Z.-M. Wang and S. Gao, *Inorg. Chem.*, 2008, **47**, 5720.

15 (*a*) Z. He, Z.-M. Wang, S. Gao and C.-H. Yan, *Inorg. Chem.*, 2006, **45**, 6694and references therein; (*b*) F.-C. Liu, Y.-F. Zeng, J.-P. Zhao, B.-W. Hu, E. C. Sañudo, J. Ribas and X.-H. Bu, *Inorg. Chem.*, 2007, **46**, 7698and references therein.

16 F.-C. Liu, Y.-F. Zeng, J.-P. Zhao, B.-W. Hu, X.-H. Bu, J. Ribas and S. R. Batten, *Inorg. Chem. Commun.*, 2007, **10**, 129.

17 *SMART*/*SAINT*Bruker AXS, Inc.: Madison, WI, 2004.

18 G. M. Sheldrick, *SHELX-97*University of Göttingen: Göttingen, Germany, 1998.

 This journal is © The Royal Society of Chemistry 2010

View Article Online

19 L. J. Farrugia, *J. Appl. Crystallogr.*, 1999, **32**, 837; L. J. Farrugia, *WinGX*, version 1.65.04; Department of Chemistry, University of Glasgow: Glasgow, Scotland, 2003.
20 (*a*) G. M. Sheldrick, *SADABS*University of Göttingen, Göttingen, Germany, 1999; (*b*) ORTEP-3 for Windows, version 1.08: L. J. Farrugia, *J. Appl. Crystallogr.*, 1997, **30**, 565.
21 V. A. Blatov, A. P. Shevchenko and V. N. Serezhkin, *Acta Crystallogr., Sect. A: Found. Crystallogr.*, 1995, **51**, 909. Also see, http://www.topos.ssu.samara.ru.
22 E. Ruiz, P. Alemany, S. Alvarez and J. Cano, *J. Am. Chem. Soc.*, 1997, **119**, 1297.
23 E. Ruiz, A. Rodríguez-Fortea, J. Cano, S. Alvarez and P. Alemany, *J. Comput. Chem.*, 2003, **24**, 982.
24 E. Ruiz, J. Cano, S. Alvarez and P. Alemany, *J. Comput. Chem.*, 1999, **20**, 1391.
25 E. Ruiz, *Struct. Bonding*, 2004, **113**, 71.
26 A. D. Becke, *J. Chem. Phys.*, 1993, **98**, 5648.
27 M. J. Frisch, G. W. Trucks, H. B. Schlegel, G. E. Scuseria, M. A. Robb, J. R. Cheeseman, J. A. Montgomery, T. Vreven, K. N. Kudin, J. C. Burant, J. M. Millam, S. S. Iyengar, J. Tomasi, V. Barone, B. Mennucci, M. Cossi, G. Scalmani, N. Rega, G. A. Petersson, H. Nakatsuji, M. Hada, M. Ehara, K. Toyota, R. Fukuda, J. Hasegawa, H. Ishida, T. Nakajima, Y. Honda, O. Kitao, H. Nakai, M. Klene, X. Li, J. E. Knox, H. P. Hratchian, J. B. Cross, C. Adamo, J. Jaramillo, R. Gomperts, R. E. Stratmann, O. Yazyev, A. J. Austin, R. Cammi, C. Pomelli, J. Ochterski, P. Y. Ayala, K. Morokuma, G. A. Voth, P. Salvador, J. J. Dannenberg, V. G. Zakrzewski, S. Dapprich, A. D. Daniels, M. C. Strain, O. Farkas, D. K. Malick, A. D. Rabuck, K. Raghavachari, J. B. Foresman, J. V. Ortiz, Q. Cui, A. G. Baboul, S. Clifford, J. Cioslowski, B. B. Stefanov, G. Liu, A. Liashenko, P. Piskorz, I. Komaromi, R. L. Martin, D. J. Fox, T. Keith, M. A. Al-Laham, C. Y. Peng, A. Nanayakkara, M. Challacombe, P. M. W. Gill, B. Johnson, W. Chen, M. W. Wong, C. Gonzalez and J. A. Pople, *Gaussian 03*, revision B.4; Gaussian Inc.: Pittsburgh, PA, 2003.
28 A. D. Becke, *Phys. Rev. A: At., Mol., Opt. Phys.*, 1988, **38**, 3098.
29 C. Lee, W. Yang and R. G. Parr, *Phys. Rev. B: Condens. Matter*, 1988, **37**, 785.
30 E. Ruiz, S. Alvarez, J. Cano and V. Polo, *J. Chem. Phys.*, 2005, **123**, 164110.
31 Z.-L. Chen, C.-F. Jiang, W.-H. Yan, F.-P. Liang and S. R. Batten, *Inorg. Chem.*, 2009, **48**, 4674.
32 A. Escuer, M. A. S. Goher, F. A. Mautner and R. Vicente, *Inorg. Chem.*, 2000, **39**, 2107.
33 Y. Song, C. Massera, M. Quesada, A. M. Manotti Lanfredi, I. Mutikainen, U. Turpeinen and J. Reedijk, *Inorg. Chim. Acta*, 2005, **358**, 1171.
34 M. H. W. Lam, Y.-T. Tang, X.-Z. You and W.-T. Wong, *Chem. Commun.*, 1997, 957.
35 J. Luo, X.-G. Zhou, S. Gao, L.-H. Weng, Z.-H. Shao, C.-M. Zhang, Y.-R. Li, J. Zhang and R.-F. Cai, *Polyhedron*, 2004, **23**, 1243.
36 T. C. Stamatatos, G. S. Papaefstathiou, L. R. MacGillivray, A. Escuer, R. Vicente, E. Ruiz and S. P. Perlepes, *Inorg. Chem.*, 2007, **46**, 8843.
37 (*a*) S. Mukherjee, B. Gole, R. Chakrabarty and P. S. Mukherjee, *Inorg. Chem.*, 2009, **48**, 11325; (*b*) K. C. Mondal and P. S. Mukherjee, *Inorg. Chem.*, 2008, **47**, 4215; (*c*) K. C. Mondal, Y. Song and P. S. Mukherjee, *Inorg. Chem.*, 2007, **46**, 9736.
38 (*a*) A. Marvilliers, S. Parsons, E. Riviere, J.-P. Audiere, M. Kurmoo and T. Mallah, *Eur. J. Inorg. Chem.*, 2001, 1287; (*b*) F. Palacio, M. Andres, R. Horne and A. J. J. van Duyneveldt, *J. Magn. Magn. Mater.*, 1986, **54–57**, 1487; (*c*) D. Cave, J.-M. Gascon, A. D. Bond, S. J. Teat and P. T. Wood, *Chem. Commun.*, 2002, 1050; (*d*) J. H. Yoon, J. H. Lim, S. W. Choi, H. C. Kim and C. S. Hong, *Inorg. Chem.*, 2007, **46**, 1529; (*e*) E.-Q. Gao, Z.-M. Wang and C.-H. Yan, *Chem. Commun.*, 2003, 1748; (*f*) Y.-G. Huang, D.-Q. Yuan, L. Pan, F.-L. Jiang, M.-Y. Wu, X.-D. Zhang, W. Wei, Q. Gao, J. Y. Lee, J. Li and M.-C. Hong, *Inorg. Chem.*, 2007, **46**, 9609; (*g*) D.-K. Cao, Y.-Z. Li and L. M. Zheng, *Inorg. Chem.*, 2007, **46**, 7571.
39 (*a*) M. E. Fisher, *Am. J. Phys.*, 1964, **32**, 343; (*b*) C. J. O'Connor, *Prog. Inorg. Chem.*, 1982, **29**, 203.
40 (*a*) A. Bencini, F. Totti, C. A. Daul, K. Doclo, P. Fantucci and V. Barone, *Inorg. Chem.*, 1997, **36**, 5022; (*b*) I. Ciofini, C. A. Daul and A. Bencini, In *Recent Advances in Density Functional Methods*, Part III; V. Barone, A. Bencini, P. Fantucci, ed.; World Scientific: Singapore, 2002.
41 J. S. Huang and M. Kertesz, *J. Am. Chem. Soc.*, 2007, **129**, 1634.
42 M. E. Ali and S. N. Datta, *J. Phys. Chem. A*, 2006, **110**, 2776.
43 E. Ruiz, J. Cirera and S. Alvarez, *Coord. Chem. Rev.*, 2005, **249**, 2649.

Published on 09 July 2010 on http://pubs.rsc.org | doi:10.1039/C0DT00181C
Downloaded by University of Chicago on 22/04/2013 15:54:28.